Numerical simulation of the motion of red blood cells and vesicles in microfluidic flows

Thomas Franke, Ronald H. W. Hoppe, Christopher Linsenmann, Lothar Schmid, Carina Willbold, Achim Wixforth

Angaben zur Veröffentlichung / Publication details:

Franke, Thomas, Ronald H. W. Hoppe, Christopher Linsenmann, Lothar Schmid, Carina Willbold, and Achim Wixforth. 2011. "Numerical simulation of the motion of red blood cells and vesicles in microfluidic flows." *Computing and Visualization in Science* 14 (4): 167–80. https://doi.org/10.1007/s00791-012-0172-1.

Numerical simulation of the motion of red blood cells and vesicles in microfluidic flows

Thomas Franke · Ronald H. W. Hoppe · Christopher Linsenmann · Lothar Schmid · Carina Willbold · Achim Wixforth

Abstract We study the mathematical modeling and numerical simulation of the motion of red blood cells (RBC) and vesicles subject to an external incompressible flow in a microchannel. RBC and vesicles are viscoelastic bodies consisting of a deformable elastic membrane enclosing an incompressible fluid. We provide an extension of the finite element immersed boundary method by Boffi and Gastaldi (Comput Struct 81:491–501, 2003), Boffi et al. (Math Mod Meth Appl Sci 17:1479–1505, 2007), Boffi et al. (Comput Struct 85:775–783, 2007) based on a model for the membrane that additionally accounts for bending energy and also consider inflow/outflow conditions for the external fluid flow. The stability analysis requires both the approximation of the membrane by cubic splines (instead of linear splines without bending energy) and an upper bound on the inflow velocity. In the fully discrete case, the resulting CFL-type condition on the time step size is also more restrictive. We perform numerical simulations for various scenarios including the tank treading motion of vesicles in microchannels, the behavior of 'healthy' and 'sick' RBC which differ by their stiffness, and the motion of RBC through thin capillaries. The simulation results are in very good agreement with experimentally available data.

Keywords Finite element immersed boundary method · Stability analysis · CFL-type condition · Red blood cells · Vesicles · Microfluidic flows

1 Introduction

Human blood is a suspension of viscoelastic cells (erythrocytes; cf. Fig. 1 (left)) in a viscous fluid (plasma). The blood flow is not only controlled by the viscosity of the plasma [26], but additionally viscoelastic effects due to the deformability of the erythrocytes [15,21], aggregation of the cells [23] and hematocrit have to be taken into account as experimentally observed in the seminal work [37] (cf. also [20,35,39,43,48,49,67,72,75–77]).

Pathologies such as cardiovascular diseases [21], malaria [70], cholesterol [19,45], diabetes mellitus [79], and liver diseases [27,54] may lead to deformations of the erythrocytes [18,32] (cf. Fig. 1 (right)) and thus change the viscoelastic properties (cf., e.g., [5,24,40]).

If not being subjected to an external flow, healthy RBC are biconcavely shaped disks with a diameter of $7.5-8.0\,\mu$m and a thickness of about $2\,\mu$m (cf. Fig. 1 (left)). However, under the influence of an external flow, the cells deform and attain parachute-like or slipper-like shapes, if being centered or decentered in the channel (cf. Fig. 2). Due to the extreme high deformability of the membrane, they can even pass through capillaries having a much smaller diameter than themselves.

Ronald H.W. Hoppe: Acknowledge support by the German National Science Foundation DFG within the Priority Programs SPP 1253 and SPP 1506, by the NSF through the grants DMS-0707602 and DMS-0914788, by the Federal Ministry for Education and Research BMBF within the research projects 'FROPT' and 'MeFreSim', and by the European Science Foundation within the Research Networking Programme 'OPTPDE'.

T. Franke · L. Schmid · A. Wixforth
Institute of Physics, University of Augsburg, 86159 Augsburg, Germany

R. H. W. Hoppe (✉)
Department of Mathematics, University of Houston, Houston, TX 77204-3008, USA
e-mail: ronald.h.w.hoppe@math.uni-augsburg.de

R. H. W. Hoppe · C. Linsenmann · C. Willbold
Institute of Mathematics, University of Augsburg, 86159 Augsburg, Germany

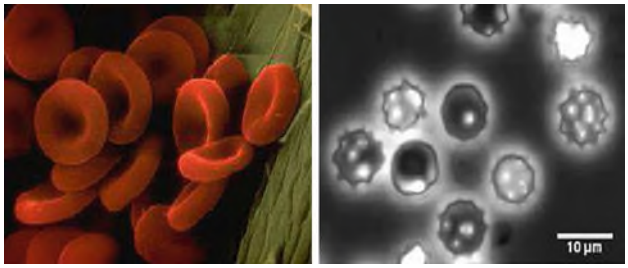

Fig. 1 Normal (*left*) and deformed (*right*) red blood cells

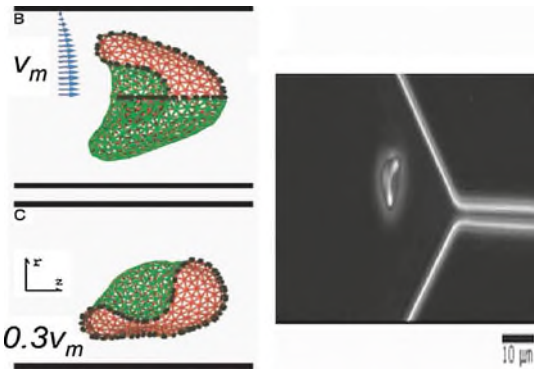

Fig. 2 Different shapes of erythrocytes in Poiseuille flow: simulation (*left*; [51]) and experiment (*right*; [16])

In contrast to healthy cells, sick RBC behave much more rigid and tend to a more swinging and tumbling behavior when exposed to an external flow.

The plasma membrane of RBC consists of a lipid bilayer membrane and an attached spectrin network as cytoskeleton [3]. Therefore, one might expect a rather complex fluidic behavior, since the underlying cytoskeleton can rearrange according to an external mechanical force [4]. However, it was demonstrated that lipid vesicles without an attached polymer network might serve as a simple model which already captures the basic physics of the fluidic problem. This also applies to some degree to liquid droplets [30].

The dynamics of vesicles in fluid flow has been studied both experimentally (see [1,2,8,22,31,41,52,53,60,61,68,80]) and theoretically (cf. [9,10,42,44,64,69]). Most of the studies were focusing on single vesicles in highly diluted suspensions. Only recently there was a rheological study presented intending to understand bulk properties from the single object properties and thus bridging the gap between the elastic properties of the objects and the viscoelastic properties of the suspension of vesicles as well as RBC (cf. [28–30,81,82]).

Various mathematical models and computational methods have been used for the numerical simulation of the motion of RBC in external flows (cf., e.g., [62] and the references therein). In particular, based on Mooney-Rivlin and Skalak models for the cell membrane, a boundary integral method has been applied in [63] to investigate the motion of RBC through thin capillaries, whereas an immersed finite element method has been implemented in [46,47] to study the rheology of RBC aggregation. Particle methods on the basis of discrete spring models for the membrane have been developed in [33,84] (lattice Boltzmann approach), in [78] (semi-implicit particle method), and in [50,51,53,65,73] (multi-particle collision dynamics). A powerful technique to simulate the motion of elastic and viscoelastic bodies in external flows is the immersed boundary method (IBM), originally developed by Peskin [56] and further studied in [14,57–59,66]. The IBM uses an Eulerian coordinate system for the flow equations and Lagrangian coordinates for the boundary of the immersed bodies together with appropriate interaction equations to transform Eulerian to Lagrangian quantities and vice versa. The interaction equations feature multidimensional Dirac delta functions that have to be approximated appropriately within a finite difference approach. For the study of the rheology of RBC in microchannels, the IBM has been applied in [6,7,35,55,83]. Recently, a variational formulation of the IBM has been provided in [11] and [12,13] as a basis for a finite element realization referred to as the finite element immersed boundary method (FE-IBM). However, these studies did not take the bending energy into account.

In this paper, we will extend the FE-IBM to the case of bending energy which has to be considered for immersed RBC or vesicles. The membrane is thus modeled as an elastic structure, but its viscous properties are neglected. We will derive the variational formulation of the problem in Sect. 2 and study its semi-discretization in space including a proper specification of the discrete elastic and bending energies in Sect. 3. Section 4 is devoted to a fully discrete approximation, and in the final Sect. 5 we report on numerical simulations of the motion of RBC in microchannels.

2 Variational formulation of the IBM

In this section, we extend the variational formulation of the IBM provided in [11] and [12] to the case of viscoelastic bodies immersed in an incompressible external fluid. The original IBM as developed in [56] relies on three groups of equations:

- the incompressible Navier-Stokes equations describing the motion of the fluid within an Eulerian coordinate system,
- the material elasticity equations describing the exerted forces of the immersed bodies in terms of the change of the total elastic energy within a Lagrangian coordinate system,
- the interaction equations which transform Eulerian into Lagrangian quantities and vice versa.

These equations are set up in a variational framework which constitutes the basis for an appropriate finite element discretization.

2.1 Incompressible Navier-Stokes equations

We assume $\Omega = (a,b)\times(c,d), a < b, c < d$, to be a domain in $\mathbb{R}^2$ with boundary $\Gamma = \overline{\Gamma}_{\text{in}} \cup \overline{\Gamma}_{\text{lat}} \cup \overline{\Gamma}_{\text{out}}$, where $\Gamma_{\text{in}} := \{a\}\times(c,d)$, $\Gamma_{\text{out}} := \{b\}\times(c,d)$, and $\Gamma_{\text{lat}} := \Gamma_{\text{bot}} \cup \Gamma_{\text{top}}$, $\Gamma_{\text{bot}} := (a,b)\times\{c\}$, $\Gamma_{\text{top}} := (a,b)\times\{d\}$. We set $Q := \Omega\times(0,T)$, $\Sigma_{\text{in}} := \Gamma_{\text{in}}\times(0,T)$, $\Sigma_{\text{lat}} := \Gamma_{\text{lat}}\times(0,T)$, $\Sigma_{\text{out}} := \Gamma_{\text{out}}\times(0,T)$, where $T > 0$. We further suppose that Ω is filled with a suspension of N viscoelastic particles immersed in an incompressible carrier fluid such that the subdomains $B_t^{(i)} \subset \Omega, 1 \le i \le N$, with $\bar{B}_t^{(i)} \cap \bar{B}_t^{(j)} = \emptyset, 1 \le i \ne j \le N$, describe the spatial location of the particles in the carrier fluid at time $t \in [0,T]$. The particles consist of an elastic membrane $\partial B_t^{(i)}$ which encloses an incompressible fluid. We assume for simplicity that both fluids have density $\rho > 0$ and viscosity $\nu > 0$. Hence, the fluid inside the membrane confers viscoelastic behavior on the immersed body. Moreover, it is incompressible such that the immersed body can only change its shape, whereas its volume is kept constant, since no-slip conditions on $\partial B_t^{(i)}$ are prescribed. We denote by $\mathbf{u} = \mathbf{u}(x,t)$ and $p = p(x,t), (x,t) \in Q$, the velocity and the pressure. We further refer to $\boldsymbol{\varepsilon}(\mathbf{u}) := (\nabla\mathbf{u} + (\nabla\mathbf{u})^T)/2$ as the rate of deformation tensor and to $\boldsymbol{\sigma}(\mathbf{u},p) := -p\,\mathbf{I} + 2\nu\boldsymbol{\varepsilon}(\mathbf{u})$ as the stress tensor. Assuming a local force density $\mathbf{F}$ in Q, periodic boundary conditions in terms of a prescribed stationary velocity $\mathbf{g}$ at the inflow boundary Σ_{in} and the outflow boundary Σ_{out}, zero velocity on Σ_{lat}, and an initial velocity $\mathbf{u}^{(0)}$ at time $t = 0$, the incompressible Navier-Stokes equations read

$$
\begin{aligned}
&\rho\Big(\frac{\partial\mathbf{u}}{\partial t} + (\mathbf{u}\cdot\nabla)\mathbf{u}\Big) - \nu\Delta\mathbf{u} + \nabla p = \mathbf{F} \text{ in } Q,\\
&\nabla\cdot\mathbf{u} = 0 \text{ in } Q,\\
&\mathbf{u} = \mathbf{g} = (g,0)^T, g \ge 0 \text{ on } \Sigma', \Sigma' \in \{\Sigma_{\text{in}}, \Sigma_{\text{out}}\},\\
&\mathbf{u} = \mathbf{0} \text{ on } \Sigma_{\text{lat}},\\
&\mathbf{u}(\cdot,0) = \mathbf{u}^{(0)} \text{ in } \Omega.
\end{aligned}
$$

In the following and throughout the rest of the paper, we use standard notation from Lebesgue and Sobolev space theory (cf., e.g., [38,74]). In particular, for a bounded domain $\Omega \subset \mathbb{R}^d, d \in \mathbb{N}$, we denote by $L^2(\Omega)$ and $\mathbf{L^2}(\Omega) := L^2(\Omega)^d$, the Hilbert space of square integrable scalar- and vector-valued functions on Ω, equipped with the inner product $(\cdot,\cdot)_{0,\Omega}$ and the associated norm $\|\cdot\|_{0,\Omega}$, respectively. $L_0^2(\Omega)$ stands for the subspace of functions with zero integral mean. Further, we denote by $\mathbf{H}^s(\Omega), s \in \mathbb{R}_+$, the Sobolev space of vector-valued functions with the inner product $(\cdot,\cdot)_{s,\Omega}$ and the associated norm $\|\cdot\|_{s,\Omega}$. The space $\mathbf{H}^s_{0,\Gamma'}(\Omega)$ is the subspace with vanishing trace on $\Gamma' \subseteq \Gamma$. We will omit the subindex Γ', if $\Gamma' = \Gamma$. $\mathbf{H}^{-s}(\Omega)$ stands for the dual space of $\mathbf{H}_0^s(\Omega)$ with $\langle\cdot,\cdot\rangle$ referring to the dual product. The space $\mathbf{H}^s(\bar{\Omega}) \subset \mathbf{H}^s(\Omega)$ is the subspace of all $\mathbf{u}|_\Omega$ where $\mathbf{u} \in \mathbf{H}^s(\mathbb{R}^d)$ and $\langle\mathbf{u}|_\Omega, \boldsymbol{\varphi}\rangle = \langle\mathbf{u}, \tilde{\boldsymbol{\varphi}}\rangle$ for all $\boldsymbol{\varphi} \in \mathbf{C}_0^\infty(\Omega)$ with $\tilde{\boldsymbol{\varphi}}$ referring to the continuation of $\boldsymbol{\varphi}$ by zero outside Ω. We denote by $\mathbf{H}^{s-1/2}(\Gamma'), s \ge 1$, the trace space of vector-valued functions on Γ'. We further refer to $\mathbf{H}_{00}^{s-1/2}(\Gamma')$ as the space of functions whose extensions by zero to $\Gamma\backslash\Gamma'$ belong to $\mathbf{H}^{s-1/2}(\Gamma)$. Finally, we denote by $C^{k,\mu}(\Omega)$ and $\mathbf{C}^{k,\mu}(\Omega), k \in \mathbb{N}_0, \mu \in (0,1/2)$, the Banach spaces of k-times continuously differentiable scalar- and vector-valued functions on Ω whose derivatives of order k are Hölder continuous of order μ.

Moreover, for $T > 0$ and a Banach space $Z(\mathbf{Z})$ of scalar (vector-valued) functions, we denote by $L^2((0,T),Z)$ ($\mathbf{L}^2((0,T),\mathbf{Z})$) the Hilbert space and by $C([0,T],Z)$ ($\mathbf{C}([0,T],\mathbf{Z})$) the Banach space of functions $v : [0,T] \to Z(\mathbf{v} : [0,T] \to \mathbf{Z})$ with norms

$$
\begin{aligned}
\|v\|_{L^2((0,T),Z)} &:= \Big(\int_0^T \|v(t)\|_Z^2 dt\Big)^{1/2},\\
\|v\|_{C([0,T],Z)} &:= \max_{t\in[0,T]} \|v(t)\|_Z,
\end{aligned}
$$

and analogous settings in the vector-valued case. The spaces $H^s((0,T),Z), s \in \mathbb{R}_+$, ($\mathbf{H}^s((0,T),\mathbf{Z})$) are defined likewise.

As far as the data of the problem are concerned, we note that the computational domain $\Omega \subset \mathbb{R}^2$ is such that for $\mathbf{v} \in \mathbf{H}^1(\Omega)$ the Poincaré-Friedrichs inequality

$$
\|\mathbf{v}\|_{0,\Omega} \le C_\Omega\Big(\|\nabla\mathbf{v}\|_{0,\Omega}^2 + \|\mathbf{v}\|_{0,\Gamma}^2\Big)^{1/2} \tag{1}
$$

holds true for some constant $C_\Omega > 0$. Moreover, we assume that $\mathbf{F}$, $\mathbf{u}^{(0)}$, and $\mathbf{g}$ satisfy

$$
\mathbf{F} \in \mathbf{L}^2((0,T),\mathbf{H}^{-1}(\Omega)), \quad \mathbf{u}^{(0)} \in \mathbf{L}^2(\Omega), \tag{2a}
$$

$$
\mathbf{g} \in \mathbf{H}_{00}^{5/2+\mu}(\Gamma_{\text{in}} \cup \Gamma_{\text{out}}), \ \mu \in (0,1/2). \tag{2b}
$$

Remark 2.1 The reason for the exponent $5/2+\mu$ in assumption (2b) is as follows: (2b) implies that the extension $\tilde{\mathbf{g}}$ of $\mathbf{g}$ by zero to the rest of Γ belongs to $\mathbf{H}^{5/2+\mu}(\Gamma)$ and satisfies (cf., e.g., [38])

$$
\|\tilde{\mathbf{g}}\|_{5/2+\mu,\Gamma} \le C_1\ \|\mathbf{g}\|_{\mathbf{H}_{00}^{5/2+\mu}(\Gamma_{\text{in}}\cup\Gamma_{\text{out}})}
$$

for some constant $C_1 > 0$. Moreover, there exists $\hat{\mathbf{g}} \in \mathbf{H}^{3+\mu}(\Omega) \cap \mathbf{H}(\text{div}^0;\Omega)$ such that $\hat{\mathbf{g}}|_\Gamma = \tilde{\mathbf{g}}$ and

$$
\|\hat{\mathbf{g}}\|_{3+\mu,\Omega} \le C_2\ \|\tilde{\mathbf{g}}\|_{5/2+\mu,\Gamma},
$$

where C_2 is a positive constant. Finally, due to the Sobolev embedding theorem [38], $\mathbf{H}^{3+\mu}(\Omega)$ is continuously embedded in $\mathbf{C}^{2,\mu}(\bar{\Omega})$, whence

$$
\|\hat{\mathbf{g}}\|_{\mathbf{C}^{2,\mu}(\bar{\Omega})} \le C_3\ \|\hat{\mathbf{g}}\|_{3+\mu,\Omega}
$$

for some constant $C_3 > 0$. Summarizing the preceding inequalities, for $\hat{C} := C_1 C_2 C_3$ we have

$$\|\hat{\mathbf{g}}\|_{\mathbf{C}^{2,\mu}(\bar{\Omega})} \leq \hat{C} \, \|\mathbf{g}\|_{\mathbf{H}_{00}^{5/2+\mu}(\Gamma_{\text{in}} \cup \Gamma_{\text{out}})}. \tag{3}$$

We introduce the function spaces

$$\begin{aligned}
&\mathbf{V}(0,T) := \mathbf{H}^1((0,T), \mathbf{H}^{-1}(\Omega)) \cap \mathbf{L}^2((0,T), \mathbf{H}^1(\Omega)),\\
&\mathbf{W}(0,T) := \{\mathbf{w} \in \mathbf{V}(0,T) \mid \mathbf{w}|_{\Sigma'} = \mathbf{g}\,,\ \mathbf{w}|_{\Sigma_{\text{lat}}} = \mathbf{0}\},\\
&Q(0,T) := L^2((0,T), L_0^2(\Omega)),
\end{aligned}$$

where $\Sigma' = \Sigma_{\text{in}} \cup \Sigma_{\text{out}}$. The weak formulation of the Navier-Stokes equations requires the computation of $(\mathbf{u}, p) \in \mathbf{W}(0,T) \times Q(0,T)$ such that for all $\mathbf{v} \in \mathbf{H}_0^1(\Omega)$ and $w \in L_0^2(\Omega)$ there holds

$$\langle \rho \frac{\partial \mathbf{u}}{\partial t}, \mathbf{v} \rangle + a(\mathbf{u}, \mathbf{v}) - b(p, \mathbf{v}) = \ell(\mathbf{v}), \tag{4a}$$

$$b(w, \mathbf{u}) = 0, \tag{4b}$$

$$\mathbf{u}(\cdot, 0) = \mathbf{u}^{(0)}. \tag{4c}$$

Here, $a(\cdot,\cdot)$, $b(\cdot,\cdot)$, and the functional $\ell(\cdot)$ are given by

$$a(\mathbf{u}, \mathbf{v}) := (\rho(\mathbf{u} \cdot \nabla)\mathbf{u}, \mathbf{v})_{0,\Omega} + (\nu \nabla \mathbf{u}, \nabla \mathbf{v})_{0,\Omega} \tag{5a}$$

$$b(p, \mathbf{v}) := (p, \nabla \cdot \mathbf{v})_{0,\Omega}, \quad \ell(\mathbf{v}) := \langle \mathbf{F}, \mathbf{v} \rangle. \tag{5b}$$

2.2 Material elasticity equations

The immersed bodies are modeled as viscoelastic bodies occupying subdomains $B_t^{(i)}$, $1 \leq i \leq N, t \in [0,T]$, such that $B_t^{(i)} \cap B_t^{(j)} = \emptyset$, $1 \leq i \neq j \leq N$, with boundaries $\partial B_t^{(i)}$ that are supposed to be non-selfintersecting closed curves. For ease of notation, we consider the case $N = 1$ and write B_t instead of $B_t^{(1)}$. The generalization to $N > 1$ is obvious. We assume that the boundary ∂B_0 of the initial configuration B_0 has length $L := |\partial B_0|$ and denote by $q \in [0, L]$ the Lagrangian coordinate labeling a material point on ∂B_0. We further refer to $\mathbf{X}(q,t) = (X_1(q,t), X_2(q,t))^T$ as the position of that point at time $t \in (0,T]$ such that

$$\mathbf{X} \in \mathbf{H}^1((0,T), \mathbf{L}^2([0,L])) \cap \mathbf{L}^2((0,T), \mathbf{H}^3_{\text{per}}([0,L])), \tag{6}$$

where $\mathbf{H}^3_{\text{per}}([0,L]) := \{\mathbf{Y} \in \mathbf{H}^3((0,L)) \mid \partial^k \mathbf{Y}(0)/\partial q^k = \partial^k \mathbf{Y}(L)/\partial q^k, k = 0,1,2\}$. We denote by

$$\mathcal{E}^e(\mathbf{X}(q,t)) = \frac{\kappa_e}{2} \left(\left| \frac{\partial \mathbf{X}}{\partial q}(q,t) \right|^2 - 1 \right), \tag{7a}$$

$$\mathcal{E}^b(\mathbf{X}(q,t)) = \frac{\kappa_b}{2} \left| \frac{\partial^2 \mathbf{X}}{\partial q^2}(q,t) \right|^2, \tag{7b}$$

the local energy densities on the immersed elastic boundary ∂B_t, where $\kappa_e > 0$ and $\kappa_b > 0$ denotes the elasticity coefficient with respect to elongation-compression and bending, respectively. Then,

$$\begin{aligned}
E(t) &:= E^e(t) + E^b(t), \quad t \in (0,T)\\
E^e(t) &:= \int_0^L \mathcal{E}^e(\mathbf{X}(q,t)) \, \mathrm{d}q,\\
E^b(t) &:= \int_0^L \mathcal{E}^b(\mathbf{X}(q,t)) \, \mathrm{d}q,
\end{aligned} \tag{8}$$

is the associated total potential energy consisting of the elastic energy $E^e(t)$ and the bending energy $E^b(t)$. The equilibrium configuration of the immersed body is that configuration for which the total energy is minimized. In case of an RBC one obtains the well known biconcave discoid [34]. The local force density $\mathbf{f}$ is given by $\mathbf{f}(q,t) = -E'(\mathbf{X}(q,t))$, where E' stands for the the Gâteaux derivative of E. We thus obtain

$$\mathbf{f}(q,t) = \kappa_e \frac{\partial^2 \mathbf{X}}{\partial q^2}(q,t) - \kappa_b \frac{\partial^4 \mathbf{X}}{\partial q^4}(q,t). \tag{9}$$

2.3 Interaction equations

In the classical IBM [56] which has been designed for finite difference discretizations, assuming $\mathbf{f}(\cdot,t) \in \mathbf{C}(\partial B_t)$ and $\mathbf{u}(\cdot,t) \in \mathbf{C}(\Omega)$ for $t \in (0,T]$, the interaction equations are given by

$$\begin{aligned}
\mathbf{F}(\mathbf{x},t) &= \int_0^L \mathbf{f}(q,t) \boldsymbol{\delta}(\mathbf{x} - \mathbf{X}(q,t)) \mathrm{d}q,\\
\frac{\partial \mathbf{X}}{\partial t}(q,t) &= \int_\Omega \mathbf{u}(\mathbf{x},t) \, \boldsymbol{\delta}(\mathbf{x} - \mathbf{X}(q,t)) \mathrm{d}\mathbf{x}.
\end{aligned}$$

Here, $\boldsymbol{\delta}(\mathbf{x}) := \delta(x_1)\delta(x_2)$ with $\delta(\cdot)$ denoting the Dirac delta function. In particular, the finite difference discretization requires an appropriate approximation of the Dirac delta function.

In the variational setting under consideration, there is no need to resort to Dirac delta functions. Assuming sufficient regularity of $\mathbf{u}(\cdot,t)$ and the test function $\mathbf{v}$, the interaction equations can be written according to

$$\langle \mathbf{F}(t), \mathbf{v} \rangle = \int_0^L \mathbf{f}(q,t) \cdot \mathbf{v}(\mathbf{X}(q,t)) \, \mathrm{d}q, \tag{10a}$$

$$\frac{\partial \mathbf{X}}{\partial t} = \mathbf{u}(\mathbf{X}(\cdot,t), t), \tag{10b}$$

$$\mathbf{X}(q,0) = \mathbf{X}^{(0)}(q), \quad q \in [0,L], \tag{10c}$$

$$\partial^k \mathbf{X}/\partial q^k(0,t) = \partial^k \mathbf{X}/\partial q^k(L,t), \quad k = 0,1,2. \tag{10d}$$

Inserting (9) into (10a), integrating by parts and observing (10d), we obtain

$$\langle \mathbf{F}(t), \mathbf{v} \rangle = -\kappa_e \int_0^L \frac{\partial \mathbf{X}(\cdot,t)}{\partial q} \cdot \frac{\partial}{\partial q} \mathbf{v}(\mathbf{X}(\cdot,t)) \mathrm{d}q$$

$$
\begin{aligned}
&-\kappa_b \int_0^L \frac{\partial^2 \mathbf{X}(\cdot,t)}{\partial q^2} \cdot \frac{\partial^2}{\partial q^2}\, \mathbf{v}(\mathbf{X}(\cdot,t))\mathrm{d}q \\
&= -\kappa_e \int_0^L \frac{\partial \mathbf{X}(\cdot,t)}{\partial q} \cdot \mathbf{D}^1\mathbf{v}(\mathbf{X}(\cdot,t))\frac{\partial \mathbf{X}(\cdot,t)}{\partial q}\, \mathrm{d}q \\
&\quad -\kappa_b \int_0^L \frac{\partial^2 \mathbf{X}(\cdot,t)}{\partial q^2} \cdot \mathbf{D}^1\mathbf{v}(\mathbf{X}(\cdot,t))\frac{\partial^2 \mathbf{X}(\cdot,t)}{\partial q^2}\, \mathrm{d}q \\
&\quad -\kappa_b \int_0^L \frac{\partial^2 \mathbf{X}(\cdot,t)}{\partial q^2} \cdot \mathbf{D}^2\mathbf{v}(\mathbf{X}(\cdot,t)) \\
&\quad \times \Big(\frac{\partial \mathbf{X}(\cdot,t)}{\partial q}, \frac{\partial \mathbf{X}(\cdot,t)}{\partial q}\Big)\mathrm{d}q. \qquad (11)
\end{aligned}
$$

Hence, as far as the test function $\mathbf{v}$ is concerned, the pointwise restriction of $\mathbf{v}$ and its first and second derivatives to ∂B_t have to be well-defined which requires $\mathbf{v}$ to be twice continuously differentiable on $\bar{B}_t$. In view of the Sobolev embedding theorem [38], this is guaranteed, if we assume $\mathbf{v} \in \mathbf{H}_0^1(\Omega) \cap \mathbf{H}^{3+\mu}(\bar{B}_t)$, $t \in [0,T]$, for some $\mu \in (0,1/2)$. On the other hand, in view of (6) and (10b) the solution $\mathbf{u} \in \mathbf{W}(0,T)$ of (4a)–(4c) also has to satisfy

$$
\mathbf{u} \in \{\mathbf{v} \in \mathbf{W}(0,T) | \mathbf{v}(\cdot,t) \in \mathbf{H}^{3+\mu}(\bar{B}_t), t \in [0,T]\}. \qquad (12)
$$

2.4 The variational IBM

Summarizing the results of the previous subsection, the variational form of the IBM requires the computation of $(\mathbf{u}, p) \in \mathbf{W}(0,T) \times Q(0,T)$ and $\mathbf{X}$ as in (6) such that $\mathbf{u}$ satisfies (12) and that for all almost all $t \in (0,T)$ and all $\mathbf{v} \in \mathbf{H}_0^1(\Omega) \cap \mathbf{H}^{3+\mu}(\bar{B}_t)$, $\mu > 0$, and all $w \in L_0^2(\Omega)$, as well as $q \in [0,L]$ there holds

$$
\begin{aligned}
&\Big\langle \rho \frac{\partial \mathbf{u}}{\partial t}, \mathbf{v} \Big\rangle + a(\mathbf{u},\mathbf{v}) - b(p,\mathbf{v}) = \ell(\mathbf{v}), && (13a)\\
&b(w,\mathbf{u}) = 0, && (13b)\\
&\mathbf{u}(\cdot,0) = \mathbf{u}^{(0)}, && (13c)\\
&\ell(\mathbf{v}) = \langle \mathbf{F}(t), \mathbf{v}\rangle, && (13d)\\
&\frac{\partial \mathbf{X}}{\partial t} = \mathbf{u}(\mathbf{X}(\cdot,t),t), && (13e)\\
&\mathbf{X}(q,0) = \mathbf{X}^{(0)}(q), && (13f)\\
&\partial^k \mathbf{X}/\partial q^k(0,t) = \partial^k \mathbf{X}/\partial q^k(L,t), \\
&k = 0,1,2. && (13g)
\end{aligned}
$$

Here, $\langle \mathbf{F}(t), \mathbf{v}\rangle$ is given by (11) and $\mathbf{X}^{(0)}$ describes the initial configuration ∂B_0 of the immersed boundary.

In case $\mathbf{u} \in \mathbf{H}^1((0,T), \mathbf{H}^{-1}(\Omega)) \cap \mathbf{L}^2((0,T), \mathbf{H}_0^1(\Omega))$ and in the absence of a bending energy, a stability result in terms of an energy estimate has been established in [12]. We will derive such an energy estimate for the problem setting under consideration which requires a restriction on the inflow/outflow velocity.

Theorem 2.1 *Let us suppose that the data of the problem* (13a)–(13g) *satisfy* (2a), (2b) *and the additional assumption*

$$
\|\mathbf{g}\|_{\mathbf{H}_{00}^{5/2+\mu}(\Gamma')} \le (8\,\rho\,\hat{C}\,C_\Omega^2)^{-1}\,\nu, \qquad (14)
$$

where $\Gamma' := \Gamma_{\mathrm{in}} \cup \Gamma_{\mathrm{out}}$ *and the positive constants* $\hat{C}, C_\Omega$ *are from* (1), (3). *Moreover, assume that the triple* $(\mathbf{u}, p, \mathbf{X})$ *satisfies* (6), (12), *and* (13a)–(13g). *Then, there exists a positive constant* C, *depending on* $\rho, \nu, \kappa_e, \kappa_b, \hat{C}$, *and* C_Ω *such that there holds*

$$
\begin{aligned}
&\frac{\rho}{4}\,\|\mathbf{u}(\cdot,t)\|_{0,\Omega}^2 + \frac{\nu}{4}\int_0^t \|\nabla \mathbf{u}(\cdot,t)\|_{0,\Omega}^2\, d\tau \\
&\quad + \frac{\kappa_e}{2}\left\|\frac{\partial \mathbf{X}(\cdot,t)}{\partial q}\right\|_{0,[0,L]}^2 + \frac{\kappa_b}{2}\left\|\frac{\partial^2 \mathbf{X}(\cdot,t)}{\partial q^2}\right\|_{0,[0,L]}^2 \\
&\le C\left(\|\mathbf{g}\|_{\mathbf{H}_{00}^{5/2+\mu}(\Gamma')} + t\,\|\mathbf{g}\|_{\mathbf{H}_{00}^{5/2+\mu}(\Gamma')}(1+\|\mathbf{g}\|_{0,\Gamma'}^2)\right. \\
&\quad + \|\mathbf{u}^{(0)}\|_{0,\Omega}^2 + \left\|\frac{\partial \mathbf{X}^{(0)}}{\partial q}\right\|_{0,[0,L]}^2 \\
&\quad + \left\|\frac{\partial^2 \mathbf{X}^{(0)}}{\partial q^2}\right\|_{0,[0,L]}^2 + \int_0^t \left\|\frac{\partial \mathbf{X}(\cdot,\tau)}{\partial q}\right\|_{0,[0,L]}^2 d\tau \\
&\quad \left. + \int_0^t \left\|\frac{\partial^2 \mathbf{X}(\cdot,\tau)}{\partial q^2}\right\|_{0,[0,L]}^2 d\tau\right). \qquad (15)
\end{aligned}
$$

Proof We recall the definition of $\hat{\mathbf{g}} \in \mathbf{H}^{3+\mu}(\Omega) \cap \mathbf{H}(\mathrm{div}^0, \Omega)$ in Remark 2.1 and choose $\mathbf{v} = \mathbf{u}(\cdot,\tau) - \hat{\mathbf{g}}$ in (13a)–(13g). Integrating over $[0,t]$, it follows that

$$
\begin{aligned}
&\int_0^t \Big\langle \rho \frac{\partial \mathbf{u}}{\partial \tau}, \mathbf{u} - \hat{\mathbf{g}} \Big\rangle\, d\tau + \int_0^t a(\mathbf{u}, \mathbf{u} - \hat{\mathbf{g}})\, \mathrm{d}\tau \\
&\quad + \frac{\kappa_e}{2}\left\|\frac{\partial \mathbf{X}(\cdot,t)}{\partial q}\right\|_{0,[0,L]}^2 + \frac{\kappa_b}{2}\left\|\frac{\partial^2 \mathbf{X}(\cdot,t)}{\partial q^2}\right\|_{0,[0,L]}^2 \\
&= \frac{\kappa_e}{2}\left\|\frac{\partial \mathbf{X}(\cdot,0)}{\partial q}\right\|_{0,[0,L]}^2 + \frac{\kappa_b}{2}\left\|\frac{\partial^2 \mathbf{X}(\cdot,0)}{\partial q^2}\right\|_{0,[0,L]}^2 \\
&\quad + \kappa_e \int_0^t \left(\frac{\partial \mathbf{X}}{\partial q}, \mathbf{D}^1\hat{\mathbf{g}}(\mathbf{X}(\cdot,\tau))\frac{\partial \mathbf{X}}{\partial q}\right)_{0,[0,L]} \mathrm{d}\tau \\
&\quad + \kappa_b \int_0^t \left(\frac{\partial^2 \mathbf{X}}{\partial q^2}, \mathbf{D}^1\hat{\mathbf{g}}(\mathbf{X}(\cdot,\tau))\frac{\partial^2 \mathbf{X}}{\partial q^2}\right)_{0,[0,L]} \mathrm{d}\tau \\
&\quad + \kappa_b \int_0^t \left(\frac{\partial^2 \mathbf{X}}{\partial q^2}, \mathbf{D}^2\hat{\mathbf{g}}(\mathbf{X}(\cdot,\tau))\left(\frac{\partial \mathbf{X}}{\partial q}, \frac{\partial \mathbf{X}}{\partial q}\right)\right)_{0,[0,L]} \mathrm{d}\tau. \qquad (16)
\end{aligned}
$$

Using the Cauchy-Schwarz inequality and Young's inequality, the first term on the left-hand side in (16) can be bounded from below according to

$$\int_0^t \left\langle \rho \frac{\partial \mathbf{u}}{\partial \tau}, \mathbf{u} - \hat{\mathbf{g}} \right\rangle d\tau \geq \frac{\rho}{4} \|\mathbf{u}(\cdot, t)\|_{0,\Omega}^2 - \rho \|\mathbf{u}(\cdot, 0)\|_{0,\Omega}^2 - \frac{3}{2} \rho \|\hat{\mathbf{g}}\|_{0,\Omega}^2. \tag{17}$$

By means of the same inequalities as well as the Poincaré-Friedrichs inequality (1), for the second term on the left-hand side in (16) we obtain

$$\begin{aligned} &\int_0^t a(\mathbf{u}, \mathbf{u} - \hat{\mathbf{g}})\, \mathrm{d}\tau \\ &\geq \left(\frac{\nu}{2} - 2\,\rho\, C_\Omega^2\, \|\hat{\mathbf{g}}\|_{C^{2,\mu}(\bar{\Omega})}\right) \int_0^t \|\nabla \mathbf{u}(\cdot, \tau)\|_{0,\Omega}^2\, \mathrm{d}\tau \\ &\quad - 2\,\rho\, C_\Omega^2\, \|\hat{\mathbf{g}}\|_{C^{2,\mu}(\bar{\Omega})} \int_0^t \|\mathbf{u}(\cdot, \tau)\|_{0,\Gamma}^2\, \mathrm{d}\tau - \frac{\nu}{2}\, t\, \|\nabla \hat{\mathbf{g}}\|_{0,\Omega}^2. \end{aligned} \tag{18}$$

The energy estimate (15) now follows by using (3), (14) in (18) and (3) in (17) as well as for the terms on the right-hand side in (16). □

3 Finite element immersed boundary method

3.1 Discretization in space

The finite element immersed boundary method (FE-IBM) is based on the a finite element discretization of the variational formulation of the IBM as given by (13a)–(13f). We assume $\mathcal{T}_h(\Omega)$ to be a simplicial triangulation of Ω that aligns with the partition of Γ. For $D \subseteq \bar{\Omega}$, we refer to $\mathcal{T}_h(D)$ as the union of triangles that have nonzero intersection with D, i.e.,

$$\mathcal{T}_h(D) = \bigcup \{K \in \mathcal{T}_h(\Omega) \mid K \cap D \neq \emptyset\}. \tag{19}$$

For $K \in \mathcal{T}_h(\Omega)$, we denote by $|K|$ the area of K and by h_K the diameter of K. We set $h := \max\{h_K \mid K \in \mathcal{T}_h(\Omega)\}$. Further, $P_k(K), k \in \mathbb{N}$, refers to the set of polynomials of degree $\leq k$ on K. We suppose that $\mathcal{T}_h(\Omega)$ is quasi-uniform, i.e., there exist constants $0 < c_Q \leq C_Q$ that only depend on the local geometry of the triangulation such that

$$c_Q h \leq h_K \leq C_Q h, \quad K \in \mathcal{T}_h(\Omega). \tag{20}$$

For the spatial discretization of the weak formulation (4a), (4b) of the incompressible Navier-Stokes equations we use P2-P1 Taylor-Hood elements [17,25], i.e., we define

$$\begin{aligned} \mathbf{V}_h &:= \{\mathbf{v}_h \in \mathbf{C}(\bar{\Omega}) | \mathbf{v}_h|_K \in P_2(K)^2,\, K \in \mathcal{T}_h(\Omega)\}, \\ Q_h &:= \{w_h \in C(\bar{\Omega}) | w_h|_K \in P_1(K),\, K \in \mathcal{T}_h(\Omega)\} \cap L_0^2(\Omega), \end{aligned}$$

and set $\mathbf{V}_{h,0} := \mathbf{V}_h \cap \mathbf{C}_0(\bar{\Omega})$. The finite element spaces $\mathbf{V}_h$ and Q_h are spanned by the canonically specified nodal basis functions.

Assuming $\mathbf{g}_h$ to be the quadratic spline interpoland of $\mathbf{g}$ with respect to $\mathcal{T}_h(\Omega)|_{\Gamma'}$, $\Gamma' = \Gamma_{\text{in}}$ resp. $\Gamma' = \Gamma_{\text{out}}$, we set

$$\begin{aligned} \mathbf{W}_h(0,T) := \{&\mathbf{w}_h \in \mathbf{C}([0,T], \mathbf{C}(\bar{\Omega})) \mid \mathbf{w}_h(\cdot, t) \in \mathbf{V}_h, \\ &\mathbf{w}_h(\cdot, t)|_{\Gamma'} = \mathbf{g}_h(\cdot), t \in [0,T]\,,\ \mathbf{w}_h|_{\Sigma_{\text{lat}}} = \mathbf{0}\}, \\ Q_h(0,T) := \{&w_h \in C([0,T]; C(\bar{\Omega})) \mid w_h(\cdot, t)|_T \in Q_h, \\ &t \in [0,T]\}. \end{aligned}$$

The discretization of the immersed boundary is done with respect to a partition

$$\mathcal{T}_{\Delta q} := \{0 =: q_0 < q_1 < \cdots < q_M := L\}, \quad M \in \mathbb{N},$$

of the interval $[0, L]$ into subintervals $I_i := [q_{i-1}, q_i]$, $1 \leq i \leq M$, of length $\Delta q_i := q_i - q_{i-1}$ with $\Delta q := \max\{\Delta q_i | 1 \leq i \leq M\}$. We approximate $\mathbf{X}$ from (6) by periodic cubic splines and thus define

$$\begin{aligned} \mathbf{S}_h := \{&\mathbf{Y}_h \in \mathbf{C}^2([0,L]; \Omega) \mid \mathbf{Y}_h|_{I_i} \in P_3(I_i)^2, \\ &1 \leq i \leq M\,,\ \mathbf{Y}_h^{(k)}(q_0) = \mathbf{Y}_h^{(k)}(q_M), \quad k = 0,1,2\}, \end{aligned}$$

where $P_3(I_i)$ stands for the set of polynomials of degree ≤ 3 on I_i. For $\mathbf{Y}_h \in \mathbf{S}_h$, we set $\mathbf{Y}_i := \mathbf{Y}_h(q_i), 0 \leq i \leq M$. We further refer to $\mathbf{D}_{\Delta q}^{\pm} \mathbf{Y}_i$ as the forward and backward difference operator as given by

$$\mathbf{D}_{\Delta q}^{+} \mathbf{Y}_i := \frac{\mathbf{Y}_{i+1} - \mathbf{Y}_i}{\Delta q_{i+1}}\,, \quad \mathbf{D}_{\Delta q}^{-} \mathbf{Y}_i := \frac{\mathbf{Y}_i - \mathbf{Y}_{i-1}}{\Delta q_i}, \tag{21}$$

and to

$$\mathbf{D}_{\Delta q}^{2} \mathbf{Y}_i := \mathbf{D}_{\Delta q}^{+} \mathbf{D}_{\Delta q}^{-} \mathbf{Y}_i \tag{22}$$

as the associated second order difference operator.

The discrete immersed body occupies subdomains $B_{h,t} \subset \Omega, t \in [0,T]$, with boundaries $\partial B_{h,t}$ that are C^2 curves described by the periodic cubic spline $\mathbf{X}_h(\cdot, t) \in \mathbf{S}_h$.

3.2 Discrete elastic energy and discrete interaction equations

We define the total discrete energy by means of

$$E_h(t) := E_h^e(t) + E_h^b(t), \tag{23}$$

where the discrete energy $E_h^e(t)$ due to elongation/compression and the discrete bending energy $E_h^b(t)$ are given by

$$E_h^e(t) = \frac{\kappa_e}{2} \int_0^L \left(\left| \frac{\partial \mathbf{X}_h}{\partial q}(q,t) \right|^2 - 1 \right) \mathrm{d}q, \tag{24a}$$

$$E_h^b(t) = \frac{\kappa_b}{2} \sum_{i=1}^{M} \int_{q_{i-1}}^{q_i} \left| \frac{\partial^2 \mathbf{X}_h}{\partial q^2}(q,t) \right|^2 \mathrm{d}q. \tag{24b}$$

Observing that $\partial^3 \mathbf{X}_h(q,t)/\partial q^3$ is constant on I_i, the discrete interaction equation takes the form

$$\begin{aligned} \langle \mathbf{F}_h(t), \mathbf{v}_h \rangle_h &= -\kappa_e \int_0^L \frac{\partial \mathbf{X}_h}{\partial q} \cdot \frac{\partial}{\partial q} \mathbf{v}_h(\mathbf{X}_h(q,t)) \mathrm{d}q \\ &\quad + \kappa_b \sum_{i=1}^{M} \int_{q_{i-1}}^{q_i} \frac{\partial^3 \mathbf{X}_h}{\partial q^3} \cdot \frac{\partial}{\partial q} \mathbf{v}_h(\mathbf{X}_h(q,t)) \mathrm{d}q \\ &= -\kappa_e \int_0^L \frac{\partial \mathbf{X}_h(q,t)}{\partial q} \cdot \nabla \mathbf{v}_h(\mathbf{X}_h(q,t)) \frac{\partial \mathbf{X}_h}{\partial q} \mathrm{d}q \\ &\quad + \kappa_b \sum_{i=1}^{M} \frac{\partial^3 \mathbf{X}_h}{\partial q^3}\Big|_{I_i} \cdot \int_{q_{i-1}}^{q_i} \nabla \mathbf{v}_h(\mathbf{X}_h(q,t)) \frac{\partial \mathbf{X}_h}{\partial q} \mathrm{d}q, \end{aligned} \tag{25}$$

which is a discrete approximation of (10a).

Remark 3.1 If we approximate $\partial B_{h,t}$ by a closed polygon with vertices in $\mathbf{X}_i(t)$, $1 \le i \le M$, the second derivatives $\partial^2 \mathbf{X}_i(t)/\partial q^2$ by the central difference quotients $\mathbf{D}^2_{\Delta q} \mathbf{X}_i(t)$ and the integrals in (24b) by the trapezoidal rule, we obtain an approximation of the discrete bending energy according to

$$E_h^b(t) \approx \frac{\kappa_b}{2} \sum_{i=1}^{M} |\mathbf{D}^2_{\Delta q} \mathbf{X}_i(t)|^2 \Delta q_i,$$

where $\mathbf{X}_{M+i} := \mathbf{X}_i$, $1 \le i \le 2$, and $\mathbf{X}_{-1} := \mathbf{X}_{M-1}$. In case $\Delta q_i = \Delta q$, $1 \le i \le M$, a simple calculation reveals

$$\begin{aligned} |\mathbf{D}^2_{\Delta q} \mathbf{X}_i(t)|^2 &= (\Delta q)^{-4} \, |(\mathbf{X}_{i+1} - \mathbf{X}_i)(t)||(\mathbf{X}_i - \mathbf{X}_{i-1})(t)| \\ &\cdot \left(\frac{|(\mathbf{X}_{i+1} - \mathbf{X}_i)(t)|}{|(\mathbf{X}_i - \mathbf{X}_{i-1})(t)|} + \frac{|(\mathbf{X}_i - \mathbf{X}_{i-1})(t)|}{|(\mathbf{X}_{i+1} - \mathbf{X}_i)(t)|} - 2\cos(\alpha_i(t)) \right), \end{aligned}$$

where $\alpha_i(t)$ is the angle formed by the vectors $(\mathbf{X}_{i+1} - \mathbf{X}_i)(t)$ and $(\mathbf{X}_i - \mathbf{X}_{i-1})(t)$, i.e.,

$$\cos(\alpha_i(t)) = \frac{(\mathbf{X}_{i+1} - \mathbf{X}_i)(t) \cdot (\mathbf{X}_i - \mathbf{X}_{i-1})(t)}{|(\mathbf{X}_{i+1} - \mathbf{X}_i)(t)||(\mathbf{X}_i - \mathbf{X}_{i-1})(t)|}.$$

Assuming $|(\mathbf{X}_{i+1} - \mathbf{X}_i)(t)| \approx |(\mathbf{X}_i - \mathbf{X}_{i-1})(t)|$ and using $\sin^2(\alpha_i(t)/2) = (1 - \cos(\alpha_i(t)))/2$, it follows that

$$\begin{aligned} |\mathbf{D}^2_{\Delta q} \mathbf{X}_i(t)|^2 &\approx 4(\Delta q)^{-4} |(\mathbf{X}_{i+1} - \mathbf{X}_i)(t)| \\ &\quad |(\mathbf{X}_i - \mathbf{X}_{i-1})(t)| \sin^2(\alpha_i(t)/2). \end{aligned}$$

Hence, introducing local bending rigidities

$$\kappa_b^{(i)} := \kappa_b \, \frac{|(\mathbf{X}_{i+1} - \mathbf{X}_i)(t)|}{\Delta q} \, \frac{|(\mathbf{X}_i - \mathbf{X}_{i-1})(t)|}{\Delta q} \cos^2(\alpha_i(t)/2),$$

we obtain

$$E_h^b(t) \approx \frac{1}{2} \sum_{i=1}^{M} \kappa_b^{(i)} \left(\frac{\tan(\alpha_i(t)/2)}{2\Delta q} \right)^2 \Delta q, \tag{26}$$

which is a frequently used approximation of the discrete bending energy (cf., e.g., [78,83]).

3.3 FE-immersed boundary method

The FE-IBM requires the computation of

$$(\mathbf{u}_h, p_h) \in \mathbf{W}_h(0,T) \times Q_h(0,T)$$

and $\mathbf{X}_h \in \mathbf{C}^1([0,T], \mathbf{S}_h)$ such that for all almost all $t \in (0,T)$ and all $\mathbf{v}_h \in \mathbf{V}_{h,0}$, $w_h \in Q_h$ there holds

$$\left\langle \rho \frac{\partial \mathbf{u}_h}{\partial t}, \mathbf{v}_h \right\rangle + a(\mathbf{u}_h, \mathbf{v}_h) - b(p_h, \mathbf{v}_h) = \ell_h(\mathbf{v}_h), \tag{27a}$$

$$b(w_h, \mathbf{u}_h) = 0, \tag{27b}$$

$$\ell_h(\mathbf{v}_h) := \langle \mathbf{F}_h(t), \mathbf{v}_h \rangle_h, \tag{27c}$$

$$\frac{\partial \mathbf{X}_h}{\partial t} = \mathbf{u}_h(\mathbf{X}_h(\cdot,t),t), \tag{27d}$$

$$\mathbf{u}_h(\cdot,0) = \mathbf{u}_h^{(0)}, \quad \mathbf{X}_h(\cdot,0) = \mathbf{X}_h^{(0)}(\cdot). \tag{27e}$$

Here, $\langle \mathbf{F}_h(t), \mathbf{v}_h \rangle_h$ is given by (25), $\mathbf{u}_h^{(0)}$ stands for the $\mathbf{L}^2$-projection of $\mathbf{u}^{(0)}$ onto $\mathbf{V}_h$ and $\mathbf{X}_h^{(0)}$ represents the initial configuration $\partial B_{h,0}$.

The following result represents the discrete counterpart of the energy norm estimate provided by Theorem 2.1. Recalling the definition of $\hat{\mathbf{g}} \in \mathbf{H}^{3+\mu}(\Omega) \subset \mathbf{C}^{2,\mu}(\bar{\Omega})$ in Remark 2.1, we define $\hat{\mathbf{g}}_h$ as the biquadratic spline interpoland of $\hat{\mathbf{g}}$ with respect to the triangulation $\mathcal{T}_h(\Omega)$ such that $\nabla \cdot \hat{\mathbf{g}}_h = 0$. In particular, there exist constants $C_{S,k} > 0$, $k \in \{0,1,2\}$, such that

$$\max_{\mathbf{x} \in \bar{\Omega}} |\mathbf{D}^k \hat{\mathbf{g}}_h(\mathbf{x})| \le C_{S,k} \|\mathbf{g}\|_{\mathbf{H}_{00}^{5/2+\mu}(\Gamma_{\mathrm{in}} \cup \Gamma_{\mathrm{out}})}. \tag{28}$$

Theorem 3.1 *In addition to the assumptions (2a), (2b) on the data suppose that*

$$\|\mathbf{g}\|_{\mathbf{H}_{00}^{5/2+\mu}(\Gamma')} \le \frac{\nu}{8 \, \rho \, C_{S,1} \, C_\Omega^2} \tag{29}$$

where $\Gamma' := \Gamma_{\mathrm{in}} \cup \Gamma_{\mathrm{out}}$ and the positive constants C_Ω, $C_{S,1}$ are from (1), (28). Moreover, assume that the triple

$$(\mathbf{u}_h, p_h, \mathbf{X}_h) \in \mathbf{W}_h(0,T) \times Q_h(0,T) \times \mathbf{C}^1([0,T]; \mathbf{S}_h)$$

satisfies (27a)–(27e). Then, there exists a positive constant C, depending on $\rho, \nu, \kappa_e, \kappa_b, C_\Omega$, and $C_{S,k}$, $0 \le k \le 2$, such that there holds

$$\frac{\rho}{4}\,\|\mathbf{u}_h(\cdot,t)\|_{0,\Omega}^2+\frac{\nu}{4}\int_0^t\|\nabla\mathbf{u}_h(\cdot,t)\|_{0,\Omega}^2\,\mathrm{d}\tau$$
$$+\frac{\kappa_e}{2}\left\|\frac{\partial\mathbf{X}_h(t)}{\partial q}\right\|_{0,[0,L]}^2+\frac{\kappa_b}{2}\left\|\frac{\partial^2\mathbf{X}_h(t)}{\partial q^2}\right\|_{0,[0,L]}^2$$
$$\le C\left((1+t)\|\mathbf{g}\|_{\mathbf{H}_{00}^{5/2+\mu}(\Gamma')}(1+\|\mathbf{g}\|_{0,\Gamma'}^2)+\|\mathbf{u}^{(0)}\|_{0,\Omega}^2\right.$$
$$+\left\|\frac{\partial\mathbf{X}_h^{(0)}}{\partial q}\right\|_{0,[0,L]}^2+\left\|\frac{\partial^2\mathbf{X}_h^{(0)}}{\partial q^2}\right\|_{0,[0,L]}^2$$
$$\left.+\int_0^t\left\|\frac{\partial\mathbf{X}_h(\tau)}{\partial q}\right\|_{0,[0,L]}^2\mathrm{d}\tau+\int_0^t\left\|\frac{\partial^2\mathbf{X}_h(\tau)}{\partial q^2}\right\|_{0,[0,L]}^2\mathrm{d}\tau\right). \tag{30}$$

Proof Choosing $\mathbf{v}_h=\mathbf{u}_h(\cdot,\tau)-\hat{\mathbf{g}}_h$ in (27a)–(27e), integrating over $[0,t]$, and using (27d), we obtain

$$\int_0^t\langle\rho\frac{\partial\mathbf{u}_h}{\partial\tau},\mathbf{u}_h-\hat{\mathbf{g}}_h\rangle\,\mathrm{d}\tau+\int_0^t a(\mathbf{u}_h,\mathbf{u}_h-\hat{\mathbf{g}}_h)\,\mathrm{d}\tau$$
$$+\frac{\kappa_e}{2}\left\|\frac{\partial\mathbf{X}_h(t)}{\partial q}\right\|_{0,[0,L]}^2+\frac{\kappa_b}{2}\left\|\frac{\partial^2\mathbf{X}_h(t)}{\partial q^2}\right\|_{0,[0,L]}^2$$
$$=\frac{\kappa_e}{2}\left\|\frac{\partial\mathbf{X}_h^{(0)}}{\partial q}\right\|_{0,[0,L]}^2+\frac{\kappa_b}{2}\left\|\frac{\partial^2\mathbf{X}_h^{(0)}}{\partial q^2}\right\|_{0,[0,L]}^2$$
$$+\kappa_e\int_0^t\int_0^L\frac{\partial\mathbf{X}_h}{\partial q}\cdot\mathbf{D}^1\hat{\mathbf{g}}_h(\mathbf{X}_h(q,\tau))\frac{\partial\mathbf{X}_h}{\partial q}\mathrm{d}q\mathrm{d}\tau$$
$$+\kappa_b\int_0^t\int_0^L\frac{\partial^2\mathbf{X}_h}{\partial q^2}\cdot\mathbf{D}^1\hat{\mathbf{g}}_h(\mathbf{X}_h(q,\tau))\frac{\partial^2\mathbf{X}_h}{\partial q^2}\mathrm{d}q\mathrm{d}\tau$$
$$+\kappa_b\int_0^t\int_0^L\frac{\partial^2\mathbf{X}_h}{\partial q^2}\cdot\mathbf{D}^2\hat{\mathbf{g}}_h(\mathbf{X}_h(q,\tau))\left(\frac{\partial\mathbf{X}_h}{\partial q},\frac{\partial\mathbf{X}_h}{\partial q}\right)\mathrm{d}q\mathrm{d}\tau. \tag{31}$$

Using the Cauchy-Schwarz inequality and Young's inequality, the first term on the left-hand side in (31) can be bounded from below according to

$$\int_0^t\left\langle\rho\frac{\partial\mathbf{u}_h}{\partial\tau},\mathbf{u}_h-\hat{\mathbf{g}}_h\right\rangle\mathrm{d}\tau\ge\frac{\rho}{4}\,\|\mathbf{u}_h(\cdot,t)\|_{0,\Omega}^2$$
$$-\rho\,\|\mathbf{u}_h(\cdot,0)\|_{0,\Omega}^2-\frac{3}{2}\,\rho\,\|\hat{\mathbf{g}}_h\|_{0,\Omega}^2. \tag{32}$$

By means of the same inequalities as well as the Poincaré-Friedrichs inequality (1) and (28), for the second term on the left-hand side in (31) we obtain

$$\int_0^t a(\mathbf{u}_h,\mathbf{u}_h-\hat{\mathbf{g}}_h)\,\mathrm{d}\tau\ge-\frac{\nu}{2}\,t\,\|\nabla\hat{\mathbf{g}}_h\|_{0,\Omega}^2$$
$$+\left(\frac{\nu}{2}-2\,\rho\,C_{S,1}C_\Omega^2\|\mathbf{g}\|_{\mathbf{H}_{00}^{5/2+\mu}(\Gamma')}\right)\int_0^t\|\nabla\mathbf{u}_h(\cdot,\tau)\|_{0,\Omega}^2\,\mathrm{d}\tau$$
$$-2\,\rho\,C_{S,1}\,C_\Omega^2\,\|\mathbf{g}\|_{\mathbf{H}_{00}^{5/2+\mu}(\Gamma')}\int_0^t\|\mathbf{u}_h(\cdot,\tau)\|_{0,\Gamma}^2\,\mathrm{d}\tau. \tag{33}$$

The energy estimate (30) now follows by similar arguments as in the proof of Theorem 3.1. □

4 Discretization in time

For the discretization in time we consider an equidistant partition

$$\mathcal{T}_{\Delta t}:=\{0=:t_0<t_1<\cdots<t_N:=T\},\quad N\in\mathbb{N},$$

of the time interval $[0,T]$ into subintervals of length $\Delta t:=T/N$. We use the forward Euler/backward Euler finite element immersed boundary method (FE/BE FE-IBM) from [12] in the sense that we discretize (27a)–(27c) in time by the backward Euler method, whereas we discretize (27d), (27e) by the forward Euler scheme. Hence, the FE/BE FE-IBM reads as follows:

Given $\mathbf{u}_h^{(0)}\in\mathbf{V}_h$ and $\mathbf{X}_h^{(0)}\in\mathbf{S}_h$, for $n=0,\dots,N-1$ we perform the following two steps:

Step 1: Compute $(\mathbf{u}_h^{(n+1)},p_h^{(n+1)})\in\mathbf{V}_h\times Q_h$ such that for all $\mathbf{v}_h\in\mathbf{V}_{h,0}$

$$(\rho\mathbf{D}_{\Delta t}^+\mathbf{u}_h^{(n)},\mathbf{v}_h)_{0,\Omega}+a(\mathbf{u}_h^{(n+1)},\mathbf{v}_h)\tag{34a}$$
$$-b(p_h^{(n+1)},\mathbf{v}_h)=\ell_h^{(n)}(\mathbf{v}_h),$$
$$b(w_h,\mathbf{u}_h^{(n+1)})=0,\tag{34b}$$
$$\ell_h^{(n)}(\mathbf{v}_h):=\langle\mathbf{F}_h^{(n)},\mathbf{v}_h\rangle_h,\tag{34c}$$

where $\langle\mathbf{F}_h^{(n)},\mathbf{v}_h\rangle_h$ is given by

$$\langle\mathbf{F}_h^{(n)},\mathbf{v}_h\rangle_h=-\kappa_e\int_0^L\frac{\partial\mathbf{X}_h^{(n)}}{\partial q}\cdot\frac{\partial}{\partial q}\mathbf{v}_h^{(n)}\mathrm{d}q$$
$$+\kappa_b\sum_{i=1}^M\int_{q_{i-1}}^{q_i}\frac{\partial^3\mathbf{X}_h^{(n)}}{\partial q^3}\cdot\frac{\partial}{\partial q}\mathbf{v}_h^{(n)}\mathrm{d}q.\tag{35}$$

Step 2: Compute $\mathbf{X}_h^{(n+1)}\in\mathbf{S}_h$ according to

$$\mathbf{D}_{\Delta t}^+\mathbf{X}_i^{(n)}=\mathbf{u}_h^{(n+1)}(\mathbf{X}_i^{(n)}),\quad 1\le i\le M.\tag{36}$$

In the proof of the energy estimate for the FE/BE FE-IBM we will frequently make use of the following partial summation result.

Lemma 4.1 *Let* $\mathbf{u} = (\mathbf{u}^{(m)})_{m=0}^{N}$ *and* $\mathbf{v} = (\mathbf{v}^{(m)})_{m=0}^{N}$ *be two vector-valued grid functions on* $\mathcal{T}_{\Delta t}$. *Then, for* $1 \le n \le N$ *there holds*

$$\sum_{m=0}^{n-1} \mathbf{D}_{\Delta t}^{+}\mathbf{u}^{(m)} \cdot \mathbf{v}^{(m)} \Delta t = -\sum_{m=1}^{n} \mathbf{u}^{(m)} \cdot \mathbf{D}_{\Delta t}^{-}\mathbf{v}^{(m)} \Delta t + \mathbf{u}^{(n)} \cdot \mathbf{v}^{(n)} - \mathbf{u}^{(0)} \cdot \mathbf{v}^{(0)}. \tag{37}$$

In particular, for $\mathbf{v} = \mathbf{u}$ *we have*

$$\sum_{m=0}^{n-1} \mathbf{D}_{\Delta t}^{+}\mathbf{u}^{(m)} \cdot \mathbf{u}^{(m)} \Delta t = \frac{1}{2}(|\mathbf{u}^{(n)}|^2 - |\mathbf{u}^{(0)}|^2). \tag{38}$$

Proof Both, (37) and (38) can be established by straightforward computation. □

The proof of the fully discrete energy estimate will require some more elementary estimates. We note that the boundary $\partial B_{h,t_n}$ of the immersed body at time t_n consists of C^2 segments $\partial B_{h,t_n}^{(i)}$ connecting the material points $\mathbf{X}_{i-1}^{(n)}$ and $\mathbf{X}_{i}^{(n)}$, $1 \le i \le M$. Recalling (19), for $K \in \mathcal{T}(\partial B_{h,t_n}^{(i)})$ we have

$$\left\| \nabla \mathbf{u}_h^{(n+1)} \right\|_{0,K\cap\partial B_{h,t_n}^{(i)}}^2 \le C_K h_K^{-1} \left\| \nabla \mathbf{u}_h^{(n+1)} \right\|_{0,K}^2,$$

where C_K is a positive constant independent of h_K. It follows that

$$\begin{aligned} \left\| \nabla \mathbf{u}_h^{(n+1)} \right\|_{0,\partial B_{h,t_n}^{(i)}}^2 &= \sum_{K\in\mathcal{T}(\partial B_{h,t_n}^{(i)})} \left\| \nabla \mathbf{u}_h^{(n+1)} \right\|_{0,K\cap\partial B_{h,t_n}^{(i)}}^2 \\ &\le \sum_{K\in\mathcal{T}(\partial B_{h,t_n}^{(i)})} C_K^2 h_K^{-1} \left\| \nabla \mathbf{u}_h^{(n+1)} \right\|_{0,K}^2. \end{aligned} \tag{39}$$

Hence, we obtain

$$\left\| \nabla \mathbf{u}_h^{(n+1)} \right\|_{0,\partial B_{h,t_n}}^2 \le C_B h^{-1} \left\| \nabla \mathbf{u}_h^{(n+1)} \right\|_{0,\Omega}^2, \tag{40}$$

where

$$C_B := c_Q^{-1} \max_{0\le n\le N-1} \max_{1\le i\le M} \left(C_i^{(n)} \max_{K\in\mathcal{T}(\partial B_{h,t_n}^{(i)})} C_K \right).$$

Here, c_Q is from (20) and $C_i^{(n)}$ denotes the maximum number of C^2 curve segments contained in an element $K \in \mathcal{T}(\partial B_{h,t_n}^{(i)})$.

In view of $\partial \mathbf{X}_h^{(n)}/\partial q \in \mathbf{C}^1([0,L]), 0 \le n \le N$, and taking into account that the third derivatives $\partial^3 \mathbf{X}_h^{(n)}/\partial q^3$ are constant vectors on I_i, $1 \le i \le M$, we further define

$$L_1 := \max_{0\le n\le N} \max_{q\in[0,L)} \left| \frac{\partial \mathbf{X}_h^{(n)}}{\partial q} \right| \Delta q, \tag{41a}$$

$$L_2 := \max_{0\le n\le N} \max_{1\le i\le M} \left| \frac{\partial^3 \mathbf{X}_h^{(n)}}{\partial q^3}|_{I_i} \right| \Delta q. \tag{41b}$$

Theorem 4.1 *In addition to the assumptions* (2a), (2b) *suppose that*

$$\|\mathbf{g}\|_{H_{00}^{5/2+\mu}(\Gamma')} \le \frac{\nu}{16\,\rho\, C_{S,1}\, C_{\Omega}^2}, \tag{42}$$

and that the following CFL-condition holds true

$$\frac{\Delta t}{h\Delta q} \le \frac{\nu}{4C_B(\kappa_e L_1 + \kappa_b L_2)}, \tag{43}$$

where $\Gamma' := \Gamma_{\text{in}} \cup \Gamma_{\text{out}}$ *and the positive constants* C_Ω, $C_{S,1}$, C_B *and* L_1, L_2 *are from* (1), (28), (40) *and* (41a), (41b). *Moreover, assume that*

$$(\mathbf{u}_h^{(n)}, p_h^{(n)}, \mathbf{X}_h^{(n)})_{n=0}^{N}$$

satisfies (34a)–(34c) *and* (35), (36). *Then, there exists a positive constant* C, *depending on* ρ, ν, κ_e, κ_b, $C_{S,k}$, $0 \le k \le 2$, *and* C_Ω, C_B, L_1, L_2 *such that it holds*

$$\begin{aligned} &\frac{\rho}{4}\|\mathbf{u}_h^{(n)}\|_{0,\Omega}^2 + \frac{\nu}{4}\sum_{m=1}^{n}\|\nabla \mathbf{u}_h^{(m)}\|_{0,\Omega}^2 \Delta t \\ &\quad + \frac{\kappa_e}{2}\left\| \frac{\partial \mathbf{X}_h^{(n)}}{\partial q} \right\|_{0,[0,L]}^2 + \frac{\kappa_b}{2}\left\| \frac{\partial^2 \mathbf{X}_h^{(n)}}{\partial q^2} \right\|_{0,[0,L]}^2 \\ &\le C\Bigg(\|\mathbf{g}\|_{\mathbf{H}_{00}^{5/2+\mu}(\Gamma')} + t\,\|\mathbf{g}\|_{\mathbf{H}_{00}^{5/2+\mu}(\Gamma')}(1 + \|\mathbf{g}\|_{0,\Gamma'}^2) \\ &\quad + \|\mathbf{u}^{(0)}\|_{0,\Omega}^2 + \left\| \frac{\partial \mathbf{X}_h^{(0)}}{\partial q} \right\|_{0,[0,L]}^2 + \left\| \frac{\partial^2 \mathbf{X}_h^{(0)}}{\partial q^2} \right\|_{0,[0,L]}^2 \\ &\quad + \sum_{m=1}^{n-1}\left\| \frac{\partial \mathbf{X}_h^{(m)}}{\partial q} \right\|_{0,[0,L]}^2 \Delta t + \sum_{m=1}^{n-1}\left\| \frac{\partial^2 \mathbf{X}_h^{(m)}}{\partial q^2} \right\|_{0,[0,L]}^2 \Delta t \Bigg). \end{aligned} \tag{44}$$

Proof We multiply (34a) by Δt and sum from $m = 0$ to $m = n-1, n \le N$, while choosing $\mathbf{v}_h = \mathbf{u}_h^{(m+1)} - \hat{\mathbf{g}}_h$ with $\hat{\mathbf{g}}_h$ as in the proof of Theorem 3.1. We thus obtain

$$\begin{aligned} &\sum_{m=0}^{n-1}\Big((\rho \mathbf{D}_{\Delta t}^{+}\mathbf{u}_h^{(m)}, \mathbf{u}_h^{(m+1)} - \hat{\mathbf{g}}_h)_{0,\Omega} \\ &\qquad + a(\mathbf{u}_h^{(m+1)}, \mathbf{u}_h^{(m+1)} - \hat{\mathbf{g}}_h)\Big)\Delta t \\ &= \sum_{m=0}^{n-1} \langle \mathbf{F}_h^{(m)}, \mathbf{u}_h^{(m+1)} - \hat{\mathbf{g}}_h \rangle_h \Delta t. \end{aligned} \tag{45}$$

Using (38) in Lemma 4.1 and Young's inequality, the first term on the left-hand side in (45) can be bounded from below as follows

$$\sum_{m=0}^{n-1}\Big(\rho\mathbf{D}^{+}_{\Delta t}\mathbf{u}_h^{(m)},\mathbf{u}_h^{(m+1)}-\hat{\mathbf{g}}_h\Big)_{0,\Omega}\,\Delta t \tag{46}$$
$$\geq\frac{\rho}{4}\,\|\mathbf{u}_h^{(n)}\|^2_{0,\Omega}-\rho\,\|\mathbf{u}_h^{(0)}\|^2_{0,\Omega}-\frac{3}{2}\rho\,\|\hat{\mathbf{g}}_h\|^2_{0,\Omega}.$$

The second term can be estimated in much the same way as in the proof of Theorem 3.1.

$$\sum_{m=0}^{n-1}a(\mathbf{u}_h^{(m+1)},\mathbf{u}_h^{(m+1)}-\hat{\mathbf{g}}_h)\Delta t\geq-\frac{\nu}{2}t_n\|\nabla\hat{\mathbf{g}}_h\|^2_{0,\Omega}$$
$$+\Big(\frac{\nu}{2}-2\rho C_{S,1}C^2_{\Omega}\|\mathbf{g}\|_{\mathbf{H}^{5/2+\mu}_{00}(\Gamma')}\Big)\sum_{m=0}^{n-1}\|\nabla\mathbf{u}_h^{(m+1)}\|^2_{0,\Omega}\Delta t$$
$$-2\rho C_{S,1}C^2_{\Omega}\|\mathbf{g}\|_{\mathbf{H}^{5/2+\mu}_{00}(\Gamma')}\sum_{m=0}^{n-1}\|\mathbf{u}_h^{(m+1)}\|^2_{0,\Gamma}\Delta t. \tag{47}$$

In view of (35) and (36), for the right-hand side in (45) we obtain

$$\sum_{m=0}^{n-1}\langle\mathbf{F}_h^{(m)},\mathbf{u}_h^{(m+1)}-\hat{\mathbf{g}}_h\rangle_h\Delta t$$
$$=-\kappa_e\sum_{m=0}^{n-1}\int_0^L\frac{\partial\mathbf{X}_h^{(m)}}{\partial q}\cdot\mathbf{D}^{+}_{\Delta t}\frac{\partial\mathbf{X}_h^{(m)}}{\partial q}\,\mathrm{d}q\,\Delta t$$
$$+\kappa_b\sum_{m=0}^{n-1}\sum_{i=1}^{M}\int_{q_{i-1}}^{q_i}\frac{\partial^3\mathbf{X}_h^{(m)}}{\partial q^3}\cdot\mathbf{D}^{+}_{\Delta t}\frac{\partial\mathbf{X}_h^{(m)}}{\partial q}\,\mathrm{d}q\,\Delta t$$
$$+\kappa_e\sum_{m=0}^{n-1}\int_0^L\frac{\partial\mathbf{X}_h^{(m)}}{\partial q}\cdot\mathbf{D}^{1}\hat{\mathbf{g}}_h\frac{\partial\mathbf{X}_h^{(m)}}{\partial q}\,\mathrm{d}q\,\Delta t$$
$$+\kappa_b\sum_{m=0}^{n-1}\int_0^L\frac{\partial^2\mathbf{X}_h^{(m)}}{\partial q^2}\cdot\mathbf{D}^{1}\hat{\mathbf{g}}_h\frac{\partial^2\mathbf{X}_h^{(m)}}{\partial q^2}\,\mathrm{d}q\,\Delta t$$
$$+\kappa_b\sum_{m=0}^{n-1}\int_0^L\frac{\partial^2\mathbf{X}_h^{(m)}}{\partial q^2}\cdot\mathbf{D}^{2}\hat{\mathbf{g}}_h\Big(\frac{\partial\mathbf{X}_h^{(m)}}{\partial q},\frac{\partial\mathbf{X}_h^{(m)}}{\partial q}\Big)\,\mathrm{d}q\,\Delta t. \tag{48}$$

Using (37) in Lemma 4.1, we find

$$-\kappa_e\sum_{m=0}^{n-1}\int_0^L\frac{\partial\mathbf{X}_h^{(m)}}{\partial q}\cdot\mathbf{D}^{+}_{\Delta t}\frac{\partial\mathbf{X}_h^{(m)}}{\partial q}\,\mathrm{d}q\,\Delta t$$
$$=+\kappa_e\sum_{m=1}^{n}\int_0^L\mathbf{D}^{-}_{\Delta t}\frac{\partial\mathbf{X}_h^{(m)}}{\partial q}\cdot\frac{\partial\mathbf{X}_h^{(m)}}{\partial q}\,\mathrm{d}q\,\Delta t$$
$$+\kappa_e\left(\int_0^L\left|\frac{\partial\mathbf{X}_h^{(0)}}{\partial q}\right|^2\mathrm{d}q-\int_0^L\left|\frac{\partial\mathbf{X}_h^{(n)}}{\partial q}\right|^2\mathrm{d}q\right). \tag{49}$$

For the first term on the right-hand side in (49) it follows that

$$\kappa_e\sum_{m=1}^{n}\int_0^L\mathbf{D}^{-}_{\Delta t}\frac{\partial\mathbf{X}_h^{(m)}}{\partial q}\cdot\frac{\partial\mathbf{X}_h^{(m)}}{\partial q}\,\mathrm{d}q\,\Delta t$$
$$=\kappa_e\sum_{m=1}^{n}\int_0^L\mathbf{D}^{+}_{\Delta t}\frac{\partial\mathbf{X}_h^{(m-1)}}{\partial q}\cdot\frac{\partial\mathbf{X}_h^{(m)}}{\partial q}\,\mathrm{d}q\,\Delta t$$
$$=\kappa_e\sum_{m=0}^{n-1}\int_0^L\mathbf{D}^{+}_{\Delta t}\frac{\partial\mathbf{X}_h^{(m)}}{\partial q}\cdot\frac{\partial\mathbf{X}_h^{(m+1)}}{\partial q}\,\mathrm{d}q\,\Delta t$$
$$=\kappa_e\sum_{m=0}^{n-1}\int_0^L\frac{\partial\mathbf{X}_h^{(m)}}{\partial q}\cdot\mathbf{D}^{+}_{\Delta t}\frac{\partial\mathbf{X}_h^{(m)}}{\partial q}\,\mathrm{d}q\,\Delta t$$
$$+\kappa_e\Delta t\sum_{m=0}^{n-1}\int_0^L\left|\mathbf{D}^{+}_{\Delta t}\frac{\partial\mathbf{X}_h^{(m)}}{\partial q}\right|^2\mathrm{d}q\,\Delta t. \tag{50}$$

Taking (36), (40), and (41a) into account, for the last term on the right-hand side in (50) we find

$$\int_0^L\left|\mathbf{D}^{+}_{\Delta t}\frac{\partial\mathbf{X}_h^{(m)}}{\partial q}\right|^2\mathrm{d}q=\int_0^L|\frac{\partial}{\partial q}(\mathbf{u}_h^{(m+1)}(\mathbf{X}_h^{(m)}))|^2\,\mathrm{d}q$$
$$\leq\int_0^L|\nabla\mathbf{u}_h^{(m+1)}(\mathbf{X}_h^{(m)})|^2\left|\frac{\partial\mathbf{X}_h^{(m)}}{\partial q}\right|\left|\frac{\partial\mathbf{X}_h^{(m)}}{\partial q}\right|\mathrm{d}q$$
$$\leq L_1(\Delta q)^{-1}\|\nabla\mathbf{u}_h^{(m+1)}\|^2_{0,\partial B_{h,t_m}}$$
$$\leq C_B L_1 h^{-1}(\Delta q)^{-1}\|\nabla\mathbf{u}_h^{(m+1)}\|^2_{0,\Omega}. \tag{51}$$

Combining (49), (50) and (51) results in

$$-\kappa_e\sum_{m=0}^{n-1}\int_0^L\frac{\partial\mathbf{X}_h^{(m)}}{\partial q}\cdot\mathbf{D}^{+}_{\Delta t}\frac{\partial\mathbf{X}_h^{(m)}}{\partial q}\,\mathrm{d}q\,\Delta t$$
$$\leq\frac{\kappa_e}{2}\left(\left\|\frac{\partial\mathbf{X}_h^{(0)}}{\partial q}\right\|^2_{[0,L]}-\left\|\frac{\partial\mathbf{X}_h^{(n)}}{\partial q}\right\|^2_{[0,L]}\right)$$
$$+\frac{\kappa_e}{2}\,C_B L_1 h^{-1}(\Delta q)^{-1}\Delta t\sum_{m=0}^{n-1}\|\nabla\mathbf{u}_h^{(m+1)}\|^2_{0,\Omega}\Delta t. \tag{52}$$

In much the same way we obtain

$$\kappa_b\sum_{m=0}^{n-1}\sum_{i=1}^{M}\int_{q_{i-1}}^{q_i}\frac{\partial^3\mathbf{X}_h^{(m)}}{\partial q^3}\cdot\mathbf{D}^{+}_{\Delta t}\frac{\partial\mathbf{X}_h^{(m)}}{\partial q}\,\mathrm{d}q\,\Delta t$$
$$\leq\frac{\kappa_b}{2}\left(\left\|\frac{\partial^2\mathbf{X}_h^{(0)}}{\partial q^2}\right\|^2_{[0,L]}-\left\|\frac{\partial^2\mathbf{X}_h^{(n)}}{\partial q^2}\right\|^2_{[0,L]}\right)$$
$$+\frac{\kappa_b}{2}\,C_B L_2 h^{-1}(\Delta q)^{-1}\Delta t\sum_{m=0}^{n-1}\|\nabla\mathbf{u}_h^{(m+1)}\|^2_{0,\Omega}\Delta t. \tag{53}$$

Observing (42) in (47) and (43) in (52), (53) and estimating the remaining terms on the right-hand side in (48) from above as in the proof of Theorem 3.1 allows to conclude. □

Remark 4.1 A comparison of the CFL-type condition (43) with that for the FE/BE FE-IBM without bending energy (cf., e.g., [12]) shows that (43) imposes a more restrictive bound on the time step size due to the impact of the bending energy.

5 Numerical results

We report on the results of three numerical simulations which demonstrate the capabilities of the FE/BE-IBM:

- tank treading effect for a vesicle subject to shear flow,
- motion of soft ('healthy') and stiff ('sick') RBC,
- flow of an RBC through a thin capillary.

We have used $\nu = 6.0 \cdot 10^{-3}$Pa · s as the viscosity of the external fluid and of the fluid enclosed by the membrane of the RBC or vesicles and considered an inflow velocity of $g = 1.0 \cdot 10^{-2}$m/s. The elastic moduli have been chosen according to $\kappa_e = 6.0 \cdot 10^{-6}$N/m and $\kappa_b = 2.0 \cdot 10^{-19}$Nm (cf. [71]). For each scenario, we have used an appropriate scaling of the underlying state equations based on data provided by our collaborating physicists. A typical magnitude of the thus determined Reynolds number $\mathrm{Re} = \rho_0 v_0 L_0/\nu_0$ is 10^{-2} which is typical for fluid flows in microchannels (the subscript 0 denotes characteristic values of the respective quantities). The implementation of the FE/BE-IBM has been done under Matlab. All computations have been performed under Linux on a work station featuring Intel Quad–CPU with 2.83 GHz each and 8 GB RAM. The computational times varied between 4 h and 48 h depending on the membrane stiffness.

5.1 Tank treading motion

A well-known phenomenon of viscoelastic particles such as vesicles or RBC in shear flow is the tank treading effect: While moving forward, the membrane of the particle rotates due to the shearing effect of the surrounding fluid, whereas its shape stays more or less the same. Tank treading is accompanied by a lift force acting on the deformed particle. In absence of other forces such as gravity, the particle will be dragged towards the center of the channel. The tank treading effect for RBC has been observed experimentally first in [36,37] and studied by the classical IBM in [34,55,83]. The measurement of the lift force is subject of ongoing experimental work in the group of T. Franke and A. Wixforth.

Figure 3 (top) shows the motion of a vesicle in shear flow by a series of snapshots from experimental data. For

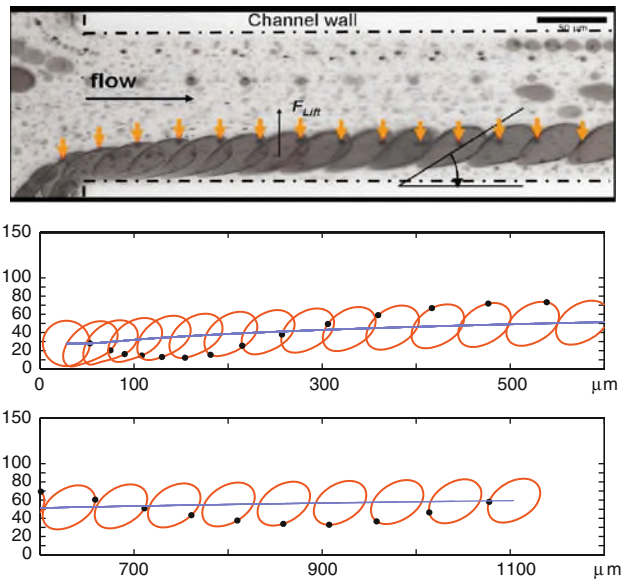

Fig. 3 Tank treading motion of an initially spherical vesicle in shear flow: series of snapshots from experimental data (*top*) and numerical simulation by the FE/BE FE-IBM (*middle* and *bottom*)

the application of the FE/BE-IBM, the underlying Navier-Stokes equations have been scaled by data from an actual experiment, allowing comparisons with the outcome of the experiment. In particular, we have used $h = \sqrt{2}/16$, $\Delta q = h/2$ ($M = 51$), resulting in a total number of degrees of freedom $DOF = 42555$, and $\Delta t = 1/240$. The results of the simulations are displayed in Fig. 3 (middle and bottom). We have also computed the inclination angle

$$\begin{aligned} &\alpha^* = \mathrm{argmax}_{\alpha\in[0,2\pi)}\ell(\alpha), \qquad (54)\\ &\ell(\alpha) := \mathrm{meas}(B_{h,t} \cap \mathbf{x}_c + t(\cos\alpha, \sin\alpha)^T),\\ &\mathbf{x}_c := \frac{1}{6\,\mathrm{meas}(B_{h,t})}\sum_{i=1}^{M} s(\mathbf{X}_i, \mathbf{X}_{i+1})(\mathbf{X}_i + \mathbf{X}_{i+1}),\\ &s(\mathbf{X}_i, \mathbf{X}_{i+1}) := X_{i,1}X_{i+1,2} - X_{i+1,1}X_{i,2} \end{aligned}$$

where $\ell(\alpha)$ denotes the length of the intersection of the vesicle and a line passing through the vesicle's center of mass $\mathbf{x}_c$ under the angle α. For given membrane nodes $\mathbf{X}_i^{(n)}$, $1 \le i \le M$, at the time instant t_n, $1 \le n \le N$, the computation of α^* requires the solution of the scalar maximization problem (54) which has been done using Matlab's `fminsearch`.

The yellow arrow in the experimental result (cf. Fig. 3 (top)) and the black dot in the simulation (cf. Fig. 3 (middle and bottom)) mark a fixed material point on the membrane. The blue line in the visualization of the simulation represents the trajectory of the center of gravity and clearly demonstrates the lift effect which is also observable in the experimental micrograph, where additionally the inclination angle is indicated. The simulations revealed an inclination angle α^* of

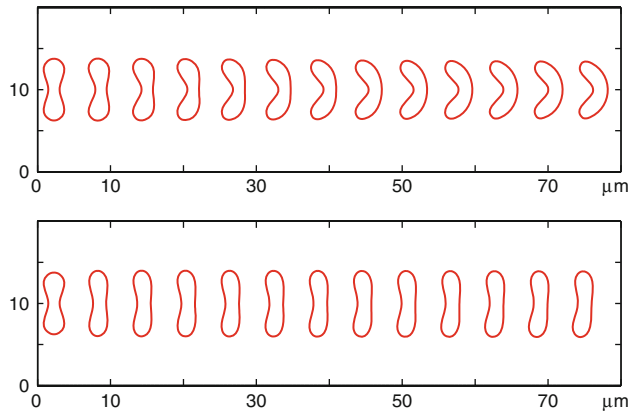

Fig. 4 Snapshots at equidistant time instants of the motion of an initially undeformed RBC in Poiseuille flow: RBC with a soft membrane (*top*) and RBC with a fifty times stiffer membrane (*bottom*)

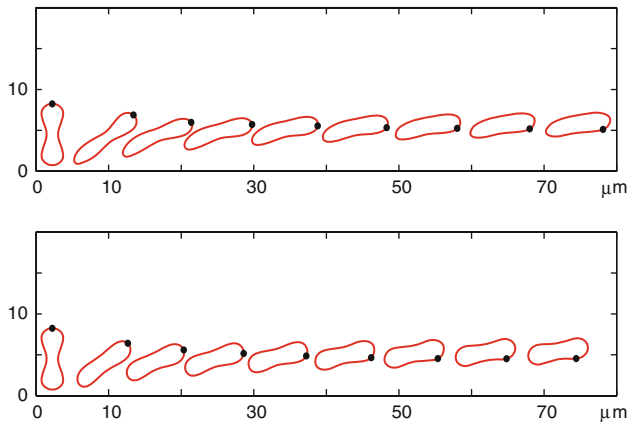

Fig. 5 Same as in Fig. 4, but now starting from a de-centered position. This leads to tank treading and a lift effect. The latter one is stronger in case of the RBC with a soft membrane

approximately 34° which is in very good agreement with the results of experimental measurements.

5.2 Effect of the membrane stiffness

As has been mentioned in Sect. 1, 'healthy' and 'sick' RBC do not show the same behavior in external flow due to a significant difference in the membrane stiffness. We have performed FE/BE-IBM simulations comparing RBC with a soft ('healthy') and a stiff ('sick') membrane.

For the stiff membrane we have chosen κ_e and κ_b fifty times larger than for the soft membrane. The initial configuration $\mathbf{X}_h(\cdot, 0)$, the typical biconcave shape of an RBC, has been obtained by performing a computation simulating the principle of minimal surface energy in a pre-processing step. We have used $h = \sqrt{2}/18$, $\Delta q = h/2$ ($M = 88$), giving $DOF = 47555$, and $\Delta t = 1/200$ (soft membrane), $\Delta t = 1/2000$ (stiff membrane). We have run two scenarios characterized by different starting positions:

In the first case, the RBC has been placed at the center of the channel (cf. Fig. 4). It can be seen that the soft RBC attains the typical parachute-like shape while passing through the channel. As expected, the stiffer RBC gets deformed less and thus also drops behind.

In the second scenario, the starting position is close to the bottom lateral wall (see Fig. 5). This leads to a deformation of the RBC due to the shearing effect of the Poiseuille flow, resulting in tank treading and lift of the RBC towards the center of the channel. The soft RBC thereby experiences stronger deformation and a stronger lift effect. The stiff RBC rotates clockwise but almost does not change its shape ('tumbling').

5.3 Motion of RBC through capillaries

It is well-known that RBC can pass through capillaries whose diameters are half or even less than the typical diameter of an RBC (7.5–8 μm), enabling oxygen supply also through highly branched blood vessels. Figure 6 (top) shows a simplified geometry for such a situation. The diameter of the microchannel varies between 20 and 4 μm. This leads to a maximal velocity inside the narrow part of the channel being almost 5 times higher than the maximal inflow velocity which results in a strong deformation of the passing RBC. We have used $h = 1/15$, $\Delta q = h/2$ ($M = 108$), giving $DOF = 26709$, and $\Delta t = 1/1000$, $T = 3.998$. The fish-like shape of the RBC inside the narrow channel is in good agreement with experimental observations (cf. Fig. 6 (bottom)).

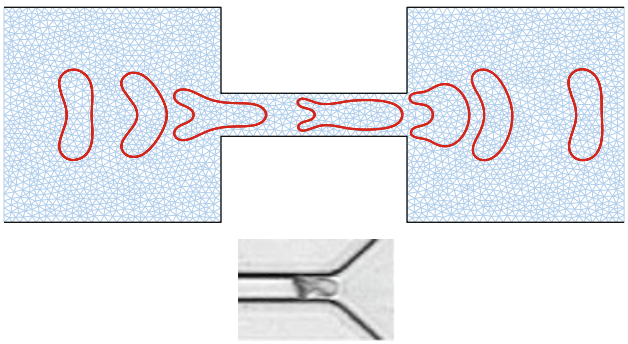

Fig. 6 Snapshots at non-equidistant time instants of a RBC passing through a channel of half its resting diameter (*top*). The comparison with an experimental result (*bottom*) reveals good coincidence with respect to the fish-like shape of the RBC inside the channel

6 Conclusions

We have extended the FE-IBM from [11–13] to the motion of viscoelastic bodies in external microchannel fluid flows by incorporating a bending energy for the membrane stiffness and by considering inflow/outflow conditions with a prescribed inflow velocity. The stability analysis reveals

that the incorporation of the bending energy requires the approximation of the boundary of the immersed bodies by cubic splines, whereas the consideration of inflow/outflow conditions leads to an upper bound on the magnitude of the inflow velocity. For the fully discrete FE/BE FE-IBM, an additional CFL-type condition on the time step size has to be satisfied which turns out to be more restrictive than in the stability analysis without bending energy.

The FE/BE FE-IBM has been applied to the numerical simulation of RBC and vesicles in shear flow with emphasis on tank treading motion, the impact of the membrane stiffness, and the motion of RBC through a thin capillary. Comparisons of the simulation results with experimentally available data show very good agreement and indicate the reliability of the approach.

Acknowledgments The authors are grateful to several useful remarks and suggestions by the referees which have led to an improvement of the exposition and the results of the paper.

References

1. Abkarian, M., Lartigue, C., Viallat, A.: Tank treading and unbinding of deformable vesicles in shear flow: determination of the lift force. Phys. Rev. Lett. **88**, 068103 (2002)
2. Abkarian, M., Viallat, A.: Dynamics of vesicles in a wall-bounded shear flow. Biophys. J. **89**, 1055 (2005)
3. Alberts, B., Johnson, A., Lewis, J., Raff, M., Roberts, K., Walter, P.: Molekularbiologie der Zelle. Weinheim, Wiley-VCH (2004)
4. An, X., Lecomte, M.C., Chasis, J.A., Mohandas, N., Gratzer, W.: Shear-response of the spectrin dimer-tetramer equilibrium in the red blood cell membrane. J. Biol. Chem. **277**(35), 31796–31800 (2002)
5. Anadere, I., Chmiel, H., Hess, H., Thurston, G.B.: Clinical blood rheology. Biorheology **16**, 171–178 (1979)
6. Bagchi, P.: Mesoscale simulation of blood flow in small vessels. Biophys. J. **92**, 1858–1877 (2007)
7. Bagchi, P., Johnson, P., Popel, A.: Computational fluid dynamic simulation of aggregation of deformable cells in a shear flow. J. Biomech. Eng. **127**, 1070–1080 (2005)
8. Baumler, H., Neu, B., Donath, E., Kiesewetter, H.: Basic phenomena of red blood cell rouleaux formation. Biorheology **36**, 439–442 (1999)
9. Beaucourt, J., Rioual, F., Seon, T., Biben, T., Misbah, C.: Steady to unsteady dynamics of a vesicle in a flow. Phys. Rev. E **69**, 011906 (2004)
10. Biben, T., Misbah, C.: Tumbling of vesicles under shear flow within an advected-field approach. Phys. Rev. E **67**, 031908 (2003)
11. Boffi, D., Gastaldi, L.: A finite element approach for the immersed boundary method. Comput. Struct. **81**, 491–501 (2003)
12. Boffi, D., Gastaldi, L., Heltai, L.: Numerical stability of the finite element immersed boundary method. Math. Mod. Meth. Appl. Sci. **17**, 1479–1505 (2007)
13. Boffi, D., Gastaldi, L., Heltai, L.: On the CFL condition for the finite element immersed boundary method. Comput. Struct. **85**, 775–783 (2007)
14. Boffi, D., Gastaldi, L., Heltai, L., Peskin, C.: On the hyper-elastic formulation of the immersed boundary method. Comput. Meth. Appl. Mech. Eng. **197**, 2210–2231 (2008)
15. Braasch, D.: Red cell deformability in capillary flow. Physiol. Rev. **51**(4), 679–701 (1971)
16. Braunmüller, S.: Viskoelastische Deformation roter Blutkörperchen. Master's Thesis. Institut für Physik, Universität Augsburg, 2007
17. Brezzi, F., Fortin, M.: Mixed and Hybrid Finite Element Methods. Springer, Berlin, Heidelberg, New York, NY (1991)
18. Chabanel, A., Chien, S., Reinhart, W.: Increased resistance to membrane deformation of shape-transformed human red blood cell. Blood **69**(3), 739 (1987)
19. Chabanel, A., Flamm, M., Sung, K.L.P., Lee, M.M., Schachter, D., Chien, S.: Influence of cholesterol content on red cell membrane viscosity and fluidity. Biophys. J. **44**, 171–176 (1983)
20. Chasis, J.A., Mohandas, N.: Erythrocyte membrane deformability and stability: two distinct membrane properties that are independently regulated by skeletal protein associations. J. Cell. Biol. **103**, 343–350 (1986)
21. Chien, S.: Red cell deformability and its relevance to blood flow. Ann. Rev. Physiol. **49**, 177 (1987)
22. Chien, S.: Shear dependence of effective cell volume as a determinant of blood viscosity. Science **168**, 977–978 (1970)
23. Chien, S., Reinhart, W.: Red cell rheology in stomatocyte-echinocyte transformation: roles of cell geometry and cell shape. Blood **67**(4), 1110 (1986)
24. Chmiel, H., Anadere, I., Walitza, E.: The determination of blood viscoelasticity in clinical hemorheology. Clin. Hemorheol. **10**, 363–374 (1990)
25. Ciarlet, P.G.: The Finite Element Method for Elliptic Problems. SIAM, Philadelphia, PA (2002)
26. Cokelet, G.R.: Rheology and hemodynamics. Ann. Rev. Physiol. **42**, 311–324 (1980)
27. Cooper, R.A.: Anemia with spur cells: a red cell defect acquired in serum and modified in the circulation. J. Clin. Inv. **48**, 1820–1831 (1969)
28. Danker, G., Biben, T., Podgorski, T., Verdier, C., Misbah, C.: Dynamics and rheology of a dilute suspension of vesicles: higher-order theory. Phys. Rev. E **76**, 041905 (2007)
29. Danker, G., Misbah, C.: Rheology of dilute suspensions of vesicles. Phys. Rev. Lett. **98**, 088104 (2007)
30. Danker, G., Verdier, C., Misbah, C.: Rheology and dynamics of vesicles suspensions in comparison with droplet emulsion. J. Non-Newtonian Fluid Mech. **152**, 156–167 (2008)
31. de Haas, K., Bloom, C., van den Ende, D., Duits, M., Mellema, J.: Deformation of giant lipid bilayer vesicles in shear flow. Phys. Rev. E **56**, 7132 (1997)
32. Dumez, H., Reinhardt, W.H., Guentes, G., de Bruijn, E.A.: Human red blood cells: rheological aspects, uptake and release of cytotoxic drugs. Crit. Rev. Clin. Lab. Sci. **41**(2), 159–188 (2004)
33. Dupin, M.M., Halliday, I., Care, C.M., Alboul, L., Munn, L.L.: Modeling the flow of dense suspensions of deformable particles in three dimensions. Phys. Rev. E **75**, 066707 (2007)
34. Eggleton, C.D., Popel, A.S.: Large deformation of red blood cell ghosts in simple shear flow. Phys. Fluids **10**, 1834–1845 (1998)
35. Evans, E.A., Fung, Y.C.: Improved measurements of the erythrocyte geometry. Microvasc. Res. **4**, 335–347 (1972)
36. Fischer, T., Schmid-Schönbein, H.: Tank treading motion of red blood cell membranes in viscometric flow: behavior of intracellular and extracellular markers. Blood Cells **3**, 351–365 (1977)
37. Fischer, T.M., Stöhr-Liesen, M., Schmid-Schönbein, H.: The red cell as a fluid droplet: tank treading-like motion of the human erythrocyte membrane in shear flow. Science **202**, 894–896 (1978)
38. Grisvard, P.: Elliptic Problems in Nonsmooth Domains. Pitman, Boston, MA (1985)
39. Hochmuth, R.M., Waugh, R.E.: Erythrocyte membrane elasticity and viscosity. Ann. Rev. Physiol. **49**, 209–219 (1987)
40. Isogai, Y., Ikemoto, S., Kuchiba, K., Ogawa, J., Yokose, T.: Abnormal blood viscoelasticity in diabetic microangiopathy. Clin. Hemorheol. **11**, 175–182 (1991)

41. Kantsler, V., Steinberg, V.: Orientation and dynamics of a vesicle in tank-treading motion in shear flow. Phys. Rev. Lett. **95**, 258101 (2005)
42. Keller, S.R., Skalak, R.: Motion of a tank-treading ellipsoidal particle in a shear flow. J. Fluid Mech. **120**, 27 (1982)
43. Khodadad, J.K., Waugh, R.E., Podolski, J.L., Steck, T.L.: Remodeling the shape of the skeleton in the intact red cell. Biophys. J. **70**, 1036–1044 (1996)
44. Kraus, M., Wintz, W., Seifert, U., Lipowsky, R.: Fluid vesicles in shear flow. Phys. Rev. Lett. **77**, 3685 (1996)
45. Lee, C.J., Kim, K., Park, H., Song, J., Lee, C.: Rheological properties of erythrocytes from male hypercholesterolemia. Microvasc. Res. **67**, 133–138 (2004)
46. Liu, W.K., Liu, Y., Farrell, D., Zhang, L., Wang, X.S., Fukui, Y., Patankar, N., Zhang, Y., Bajaj, C., Lee, J., Hong, J., Chen, X., Hsu, H.: Immersed finite element method and its applications to biological methods. Comput. Methods Appl. Mech. Eng. **195**, 1722–1749 (2006)
47. Liu, W.K., Liu, Y.: Rheology of red blood cell aggregates by computer simulation. J. Comp. Phys. **220**, 139–154 (2006)
48. Marascalco, P.J., Ritchie, S.P., Snyder, T.A., Kameneva, M.V.: Development of standard tests to examine viscoelastic properties of blood of experimental animals for pediatric mechanical support device evaluation. ASAIO **52**, 567–574 (2006)
49. More, R.B., Thurston, G.B.: Intrinsic viscoelasticity of blood cell suspensions: effects of erythrocyte deformability. Biorheology **24**, 297–309 (1987)
50. Noguchi, H., Gompper, G.: Fluid vesicles with viscous membranes in shear flow. Phy. Rev. Lett. **93**, 258102 (2004)
51. Noguchi, H., Gompper, G.: Shape transitions of fluid vesicles and red blood cells in capillary flows. Proc. Nat. Acad. Sci. USA **102**, 14159–14164 (2005)
52. Noguchi, H., Gompper, G.: Swinging and tumbling of fluid vesicles in shear flow. Phys. Rev. Lett. **98**, 128103 (2007)
53. Noguchi, H., Gompper, G., Schmid, L., Wixforth, A., Franke, T.: Dynamics of fluid vesicles in flow through structured microchannels. Eur. Phys. Lett. **89**, 28002 (2010)
54. Owen, J.S., Brown, D.J.C., Harry, D.S., Mcintyre, N.: Erythrocyte echinocytosis in liver disease: role of abnormal plasma high density llipoproteins. J. Clin. Inv. **76**, 2275–2285 (1985)
55. Pan, T.-W., Wang, T.: Dynamical simulation of red blood cell rheology in microvessels. Int. J. Numer. Anal. Model. **6**, 455–473 (2009)
56. Peskin, C.: Numerical analysis of flood flow in the heart. J. Comput. Phys. **25**, 220–252 (1977)
57. Peskin, C.: The immersed boundary method. Acta Numerica **11**, 479–517 (2002)
58. Peskin, C., McQueen, D.M.: A three-dimensional computational method for blood flow in the heart. I. Immersed elastic fibers in a viscous incompressible fluid. J. Comput. Phys. **81**, 372–405 (1989)
59. Peskin, C., Printz, B.F.: Improved volume conservation in the computation of flows with immersed elastic boundaries. J. Comput. Phys. **105**, 33–46 (1993)
60. Pozrikidis, C.: Finite deformation of liquid capsules enclosed by elastic membranes in simple shear flow. J. Fluid Mech. **297**, 123–152 (1995)
61. Pozrikidis, C.: Effect of membrane bending stiffness on the deformation of capsules in simple shear flow. J. Fluid Mech. **440**, 269–291 (2001)
62. Pozrikidis, C.: Modeling and Simulation of Capsules and Biological Cells. Chapman & Hall/CRC, Boca Raton, FL (2003)
63. Pozrikidis, C.: Axisymmetric motion of a file of red blood cells through capillaries. Phys. Fluids **17**, 031503 (2005)
64. Rioual, F., Biben, T., Misbah, C.: Analytical analysis of a vesicle tumbling under a shear flow. Phys. Rev. E **69**, 061914 (2004)
65. Ripoli, M., Mussawisade, K., Winkler, R.G., Gompper, G.: Low-Reynolds-number hydrodynamics of complex fluids by multi-particle-collision dynamics. Europhys. Lett. **68**, 106–112 (2004)
66. Rosar, M.E., Peskin, C.S.: Fluid flow in collapsible elastic tubes: a three-dimensional numerical model. N. Y. J. Math. **7**, 281–302 (2001)
67. Secomb, T.W., Hsu, R.: Analysis of red blood cell motion through cylindrical micropores: effects of cell properties. Biophys. J. **71**, 1095–1101 (1996)
68. Seifert, U.: Hydrodynamic lift on bound vesicles. Phys. Rev. Lett. **83**, 876–879 (1999)
69. Seifert, U.: Fluid membranes in hydrodynamic flow fields: formalism and an application to fluctuating quasispherical vesicles in shear flow. Eur. Phys. J. B **8**, 405 (1999)
70. Shelby, P., Rathod, P.K., Ganesan, K., Whiteand, J.M., Chiu, D.T.: A microfluidic model for single-cell capillary obstruction by plasmodium falciparum-infected erythrocytes. PNAS **100**(25), 114618–114622 (2003)
71. Skalak, R., Chien, S.: Handbook of Bioengineering. McGraw-Hill, New York, NY (1987)
72. Stoltz, J., Singh, M., Riha, P.: Hemorheology in Practice. IOS Press, Amsterdam (1999)
73. Tao, Y.-G., Götze, I.O., Gompper, G.: Multiparticle collision dynamics modeling of viscoelastic fluids. J. Chem. Phys. **128**, 144902 (2008)
74. Tartar, L.: Introduction to Sobolev Spaces and Interpolation Theory. Springer, Berlin, Heidelberg, New York, NY (2007)
75. Thurston, G.B.: Viscoelasticity of human blood. Biophys. J. **12**, 1205–1217 (1972)
76. Thurston, G.B.: Effects of viscoelasticity of blood on wave propagation in the circulation. J. Biomech. **9**, 13–20 (1976)
77. Thurston, G.B.: Viscoelastic properties of blood and blood analogs. In: Hoew, T.C. (ed.) Advances in Hemodynamics and Hemorheology, pp. 1–30. JAI Press, Greenwich (1996)
78. Tsubota, K., Wada, S., Yamaguchi, T.: Simulation study on effects of hematocrit on blood flow properties using particle method. J. Biomech. Sci. Eng. **1**, 159–170 (2006)
79. Tsukada, K., Minamitani, H., Oshio, C., Sekizuka, E.: Direct measurement of erythrocyte deformability in diabetes mellitus with a transparent microchannel capillary model and high speed video camera system. Microvasc. Res. **61**, 231–239 (2001)
80. Vitkova, V., Mader, M., Biben, T., Podgorski, T.: Tumbling of lipid vesicles, enclosing a viscous fluid, under a shear flow. J. Optoelectr. Adv. Mater. **7**, 261 (2005)
81. Vitkova, V., Mader, M., Misbah, C., Podgorski, T.: Rheology of dilute suspensions of vesicles and red blood cells. arXiv:0704.4287vl[cond-mat.soft] (2007)
82. Vitkova, V., Mader, M., Polack, B., Misbah, C., Podgorski, T.: Micro-macro link in rheology of erythrocyte and vesicle suspensions. Biophys. J. **95**, L33–L35 (2008)
83. Wang, T., Pan, T.-W., Xing, Z.W., Glowinski, R.: Numerical simulation of red blood cell rouleaus in microchannels. Phys. Rev. E **79**, 041916-1–041916-11 (2009)
84. Zhang, J., Johnson, P.C., Popel, A.S.: Red blood cell aggregation and dissociation in shear flows simulated by the lattice Boltzmann method. J. Biomech. **41**, 47–55 (2008)